Modelling the Fragmentation of Protostellar Cores With Ambipolar Diffusion

by

Christopher Thomas MacMackin

A THESIS SUBMITTED IN PARTIAL FULFILMENT OF
THE REQUIREMENTS FOR THE DEGREE OF

BACHELOR OF SCIENCE

in

Honours Astrophysics

(Department of Astronomy and Physics, Dr. David A. Clarke supervising faculty)

....
....
....
....
....

SAINT MARY'S UNIVERSITY

June 9, 2015

Abstract

Modelling the Fragmentation of Protostellar Cores With

Ambipolar Diffusion

by *Christopher Thomas MacMackin*

submitted on June 9, 2015:

Most stars are observed in multiple star systems, which are thought to result from the fragmentation of a protostellar cores as they collapse. This process has been studied extensively using numerical simulations but, to date, relatively few of these account for the effects of magnetic fields. Of those that do, almost all work under the assumption of ideal magnetohydrodynamics (i.e. the gas is completely ionized). However, the gas in a protostellar core would only be very weakly ionized and would thus tend to drift relative to magnetic field lines, in a process called ambipolar diffusion. In this thesis, an attempt was made to implement ambipolar diffusion in the *ZEUS-3D* magnetohydrodynamics code, so as to investigate the effects of ambipolar diffusion on the fragmentation process. While the implementation worked well for 1D tests, it was found to produce instabilities when run in 3D while solving for total energy. Simulations could be run without instabilities when solving for internal energy, but ambipolar diffusion required such a small time-step as to make all but the lowest resolution simulations impractical. What simulations could be run indicated that ambipolar diffusion does, indeed, produce noticeably different results from those obtained with ideal MHD or ignoring magnetic fields altogether.

Contents

List of Figures

List of Tables

Chapter 1

STAR FORMATION AND FRAGMENTATION

Star formation is an area of great interest in astrophysics. Both empirical and theoretical evidence indicates that stars collapse from interstellar gas clouds. These clouds exist on a hierarchy of scales, ranging from Giant Molecular Clouds (with diameters of order 10^1–10^2 pc and masses of order 10^5–10^6 $M_\odot$) to pre-stellar cores (with diameters of order 0.01–0.1 pc and masses of order $1 M_\odot$). It is these cores which will ultimately collapse into a single star system (Pudritz, 2001).

It has also been observed that the majority of stars exist within multi-body systems (Goodwin et al., 2007). Exactly how such systems form has been a matter of some debate. It is now considered unlikely that companion stars are captured during an encounter with larger stars (Boss, 1993) and the favoured mechanism is that these stars formed in multiple star systems (Boss, 2002; Goodwin et al., 2007). This would require the pre-stellar cores to fragment at some point during their collapse.

1.1 Collapse and Fragmentation Physics

1.1.1 The Jeans Length and Mass

Cores are supported by thermodynamic pressure, magnetic fields and rotation. On the other hand, gravity tends to pull the gas inwards on itself. The cloud can only collapse if the force of gravity is able to overcome the force from pressure (and any other forces). Neglecting magnetism and rotation for the time being, whether or not a cloud will collapse can be quantified by the Jeans mass, M_{J}, and Jeans length, λ_{J} (Carroll and Ostlie, 2007).

Following the method used by Carroll and Ostlie (2007), the Jeans mass and length can be derived as follows. The virial theorem states that if a system is stable against collapse and expansion,

$$2K + U = 0, \tag{1.1}$$

where K and U are kinetic and potential energy, respectively. If a gas cloud is a sphere of radius R_{c} and mass M_{c}, with uniform density, then

$$U = \frac{3}{5}\frac{GM_{\mathrm{c}}^2}{R_{\mathrm{c}}}. \tag{1.2}$$

From thermodynamics, we can say that the cloud's internal kinetic energy is

$$K = \frac{3}{2}NkT, \tag{1.3}$$

where N is the number of particles in the cloud, k is the Boltzmann constant, and T is the cloud's temperature. If the average molecular weight of a particle in the cloud is μ, then that means

$$N = \frac{M_\mathrm{c}}{\mu m_\mathrm{H}}, \tag{1.4}$$

where m_H is the mass of a Hydrogen atom.

If the cloud is to collapse, the virial theorem requires that $2K < |U|$, or

$$\frac{3M_\mathrm{c}kT}{\mu m_\mathrm{H}} < \frac{3}{5}\frac{GM_\mathrm{c}^2}{R_\mathrm{c}}. \tag{1.5}$$

If the cloud initially has a density ρ_0, then

$$R_\mathrm{c} = \left(\frac{3M_\mathrm{c}}{4\pi\rho_0}\right)^{1/3} \tag{1.6}$$

which, when substituted into Equation (1.5), yields

$$\frac{kT}{\mu m_\mathrm{H}} < \frac{1}{5}GM_\mathrm{c}^{2/3}\left(\frac{4}{3}\pi\rho_0\right)^{1/3}. \tag{1.7}$$

In order for the gas cloud to collapse, then, its mass (M_c) must be greater than the Jeans mass:

$$M_\mathrm{c} > M_\mathrm{J} \equiv \left(\frac{5kT}{G\mu m_\mathrm{H}}\right)^{3/2}\left(\frac{3}{4\pi\rho_0}\right)^{1/2}. \tag{1.8}$$

Rearranging Equation (1.6) to

$$M_\mathrm{c} = \frac{4}{3}\pi R_\mathrm{c}^3\rho_0 \tag{1.9}$$

and substituting it into Equation (1.5) yields the Jeans length,

$$R_{\mathrm{J}} = \left(\frac{15kT}{4\pi G \mu m_{\mathrm{H}} \rho_0} \right)^{1/2}. \tag{1.10}$$

As with the Jeans mass, if a cloud has a radius greater than the Jeans length it will collapse under its own gravity. If a cloud has a lower mass or radius than the Jeans values, however, it will be stable against collapse.

If a pre-stellar core were perfectly spherical and homogeneous then it would collapse smoothly until radiation from the liberated potential energy of incoming gas and from nuclear fusion provided sufficient thermal pressure to counterbalance gravity. This would result in the formation of a single star. As the cloud collapsed its density would grow, further reducing its Jeans mass/length and allowing it to collapse even faster. Real clouds are never so uniform and will always have over- and under-dense regions within them. As the densities of these over-dense regions increases, their Jeans mass will decrease. Eventually it may decrease sufficiently as to be lower than the mass of this portion of the cloud. In this case, this over-dense region can begin collapsing independently from, and more rapidly than, the rest of the cloud. These over-dense regions will thus be able to form separate stars in a multi-star system (Hoyle, 1953; Hunter, 1962). This process is called "fragmentation". Fragmentation can occur multiple times within a core and can also occur again within fragments themselves.

It can be shown (see, for example, Carroll and Ostlie, 2007) that the time which it would take for a uniform cloud to collapse to a point if there was no appreciable

pressure, rotation, magnetism, or turbulence supporting it is

$$t_{\mathrm{ff}} = \sqrt{\frac{3\pi}{32 G \rho_0}}. \tag{1.11}$$

Although such conditions will never be true throughout the collapse of a gas cloud, this "free-fall time" remains useful, as it is of the same order of magnitude as the actual collapse time. Thus, it is a common way to express the progress in simulations of star formation.

1.1.2 Magnetism and Ambipolar Diffusion

In addition to thermal pressure, magnetic fields can also support gas clouds against collapse. If the magnetic fields are coupled to the gas then their strength will increase as the cloud collapses. This, in turn, increases magnetic pressure and tends to impede further collapse. Ignoring thermal energy for the moment, the virial theorem can be applied using the potential energy stored in the magnetic field. In this case, the Jeans mass can be derived to be

$$M_{\mathrm{B}} = c_{\mathrm{B}} \frac{\pi R^2 B}{G^{1/2}}, \tag{1.12}$$

where $c_B = 380 \mathrm{N}^{1/2} \mathrm{m}^{-1} \mathrm{T}^{-1}$ for a uniform, spherical cloud and B is the magnetic field strength (Carroll and Ostlie, 2007). If a cloud's mass is less than M_B then it stable against collapse and said to be magnetically subcritical. If, however, its mass is greater than M_B then it can collapse and is said to be magnetically supercritical. However, it may still be possible for thermal pressure to support the cloud against

gravity.

Initially, magnetic fields have the potential to make it quite difficult for clouds to collapse, as magnetic pressure supports the cloud against gravity. However, magnetic breaking can rob a cloud of nearly all of its angular momentum. This makes it easier for the cloud to collapse, but hinders or prevents the process of fragmentation (see §1.3). This is known as the "magnetic breaking catastrophe" (Li et al., 2014).

One effect which may help to overcome these issues is ambipolar diffusion. Most magnetohydrodynamics (MHD) simulations assume that the gas is entirely ionized (so-called "ideal MHD"). However, most of the gas in pre-stellar cores is neutral. This gas will not be directly affected by magnetic fields, which only influence the motion of charged particles (ions). The reason that ideal MHD can be applicable in such a situation is that the neutral particles will collide with the ionized ones. These collisions allow the ions effectively to "drag" the neutral particles along with them. However, in reality, the coupling between these two components of the gas is not perfect (see §2.2 and §2.3 for a detailed discussion of how this affects the equations for MHD). If there is a preferred direction to the motion of the neutral gas (i.e. due to a gravitational potential), it will tend to "slip" relative to the magnetic field. Thus, collapse and fragmentation could still occur, albeit more slowly than had the magnetic field been absent entirely (Carroll and Ostlie, 2007).

1.2 Parameters

The initial conditions of core-collapse simulations are typically described using two parameters: α and β (see, for example, Boss, 1993). The former is the initial ratio of thermal to gravitation potential energy within the core, while the latter is the ratio of rotational to gravitational potential energy.

$$\alpha = \frac{5}{2} \left(\frac{3}{4\pi \rho_0 M_c^2} \right)^{1/3} \frac{c_s^2}{G} \tag{1.13}$$

$$\beta = \frac{1}{4\pi} \frac{\Omega^2}{G\rho_0} \tag{1.14}$$

where $c_s = \sqrt{p/\rho}$ is the isothermal sound speed and Ω is the angular frequency of the cloud's rotation. Both thermal and rotational energy impede collapse. Thermal energy results in higher pressure, which resists the force of gravity. Rotation requires that some of the gravitation force be used to provide a centripetal force and will not be able to contribute to the cloud's tendency to collapse.

Most magnetohydrodynamics (MHD) simulation use a different approach to quantify the relative strength of the magnetic field than we see for thermal and rotational energies. This is the mass-to-flux ratio, $\Gamma \equiv M/\Phi$ (Hosking and Whitworth, 2004):

$$\Gamma = 1.25 \times 10^{-3} \sqrt{\frac{G\mu_0}{\pi}} \frac{M_c}{\pi R_c^2 B} \tag{1.15}$$

Cores with $\Gamma > 1$ are said to be magnetically "supercritical" and are capable of

collapsing, although not necessarily fragmenting, while those with $\Gamma < 1$ are called "magnetically subcritical" and are supported against collapse by the magnetic field. However, here the choice was made to use a parameterization more in keeping with that for thermal and rotational energy. The ratio of magnetic to gravitational potential energy in the cloud is expressed using

$$\zeta_{\mathrm{m}} = \frac{5B^2}{6G\mu_0} \left(\frac{3}{4\pi \rho_0 M_{\mathrm{c}}^5} \right)^{(1/3)}.$$ (1.16)

Most simulations are initialized with a spherical gas cloud of uniform density. As mentioned earlier, such a system will not fragment. It is therefore necessary to give it a perturbation. Various types of perturbations may be used, but perhaps the most common is an azimuthal perturbation of the form

$$\delta\rho = \rho_0(1 + A\cos(m\phi)),$$

where m is the mode of the perturbation and A is its amplitude. Typically, m is chosen to be two (bifurcation) while A is chosen to be 0.1.

1.3 Early Simulations

Due to the complexity of the problem, most theoretical work on star formation is done via numerical simulations, the approach taken within this thesis. An overview of previous research is provided below.

The first simulations of star formation were purely hydrodynamical and neglected

the effects of magnetic fields. The earliest 3D computer simulations of star formation known to this author were performed by Larson (1978) using a Lagrangian approach (effectively an early smoothed particle hydrodynamics, or SPH, code). The simulations were initialized by randomly spreading the desired number of particles within a spherical volume. This research showed that fragmentation readily occurred if the mass of the initial gas cloud were greater than the Jeans mass. Furthermore, the number of objects which ultimately formed tended to be similar to the number of Jeans masses initially present.

Subsequent work by Boss and Bodenheimer (1979) agreed with these results. Boss and Bodenheimer ran simulations using two separate finite-difference codes, one with a spherical and the other with a cylindrical grid geometry. The initial conditions were those of a uniform spherical gas cloud of $1\mathrm{M}_\odot$ with a density perturbation of the form $\rho = \rho_0[1 + A\sin(m\phi)]$ where $A = 0.5$ and $m = 2$. Both simulations produced qualitatively similar results, demonstrating fragmentation of the gas cloud.

However, a paper by Tohline (1980a) suggested that fragmentation did not occur so easily after all. Also using a finite-difference code, Tohline found that a gas cloud would fragment only if some of the initial perturbations were Jeans unstable from the start. A subsequent paper (Tohline, 1980b) provided theoretical justification for this behaviour. Other initializations tended to produce ring structures which were stable against fragmentation. Stable ring structures are unusual because rings normally fragment, as in Boss (2002). Tohline, 1980a acknowledges this peculiarity and shows that the stability of these rings arises due to a quirk of the evolutionary path they followed.

In another study, Boss (1993) tracked the evolution of rotating ellipsoidal clouds with Gaussian density profiles. A range of behaviours were observed which could be divided into three categories: failure to collapse altogether; collapse into a single object; and fragmentation into a binary system or the formation of a bar structure which was expected to undergo fragmentation in the future.

However, doubt was cast on many of these earlier works demonstrating fragmentation when a hitherto unknown numerical artifact which artificially promoted fragmentation was discovered.

1.4   The Jeans Condition

This artifact, which applied to self-gravitating simulations, was discovered in 1997 by Truelove et al. All numerical simulations feature some errors as a result of descretization, which must be kept small if the simulation is to be useful. However, these errors can produce perturbations which, due to gravity, will attract more mass. This causes the perturbations to grow still more dense, increasing the inward pull of gravity, creating a vicious cycle. Effectively, these ever-growing perturbations cause the cloud to fragment. This "artificial fragmentation" does not correspond to any physical process but can give the false impression that a gas cloud is fragmenting when, in fact, it should not. In extreme cases, it was found that this instability caused fragmentation to occur in simulations initialized without any seed.

Truelove et al. (1997) found that, with sufficiently fine resolution, they were able to avoid any numerical errors large enough to cause artificial fragmentation. They

described resolution using a quantity which they named the Jeans number:

$$J \equiv \frac{\Delta x}{\lambda_J} \qquad (1.17)$$

where Δx is the size of a zone in the simulation and λ_J is the Jeans length for the fluid within that zone. Through experimentation, Truelove et al. found that they needed

$$J < 0.25 \qquad (1.18)$$

in order to prevent artificial fragmentation. Equation (1.18) is known as the Jeans condition and it is necessary, although not always sufficient, that simulation respect it if the results are to be reliable. This can be best achieved using adaptive mesh refinement, or AMR, (Berger and Oliger, 1984; Berger and Colella, 1989) as was done by Truelove et al. themselves (1997; 1998). AMR will increase the resolution of the simulation grid where it is needed and reduce it where it is not. This has the advantage that simulations will be accurate but will not use resources where it is unnecessary to do so. A simpler, although less effective, alternative is to use a nonuniform grid, which will have higher resolution in regions where high densities are expected.

While obeying the Jeans condition does prevent some fragmentation (i.e. that which is a numerical artifact), fragmentation is certainly still possible, as was demonstrated in Truelove et al.'s 1997 paper. It was found there that a gas cloud with a Gaussian radial profile and a 10% $m = 2$ perturbation—similar to that used by Boss

and Bodenheimer (1979)—would collapse into two filamentary fragments. Similarly, a 1998 paper by the same authors found that a uniform cloud with either a 10 or 50% $m = 2$ perturbation would also form to filamentary fragments, although with a somewhat different orientation towards each other. The latter initialization has become something of a standard test for fluid codes with self-gravity.

1.5 MHD Simulations

While there has been a great deal of work done simulating star formation, relatively little of it has incorporated magnetic fields. This is, in large part, due to the more difficult nature of MHD compared to ordinary fluid dynamics. A few ideal MHD simulations were performed in the 1980s using both finite difference (Dorfi, 1982) and SPH (Benz, 1984) algorithms. Both observed that magnetic fields dramatically reduced the angular momentum present in the clouds, and the former also noted that collapse was strongly inhibited. Two papers by Phillips (1986a; 1986b) using an SPH code did observe collapse with a magnetic field but no fragmentation, even when perturbations were applied to the initial density distribution. Note, however this was at least partly due to the simulated clouds being non-rotating, as fragmentation was difficult to achieve for these parameters even when magnetic fields were absent (Boss, 1997).

The first attempt to model magnetic fields in three-dimensional star-formation simulations with ambipolar diffusion was by Boss (1997, 2000, 2002). However, this was not a proper MHD simulation and worked on the basis of parameterizing magnetic

field strength and then altering the gravitational acceleration to account for magnetic pressure and tension. This approach is incapable of dealing with any transverse forces and will miss many of the effects of magnetism, such as magnetic breaking.

Boss also includes a crude model of ambipolar diffusion (see Section 2.2). Boss cites three papers which he feels indicate that ambipolar diffusion, by reducing the magnetic field strength, makes magnetic braking insignificant, although the work of (Hosking and Whitworth, 2004) would seem to contradict this assertion. Surprisingly, Boss found that including magnetic fields actually seemed to aid in fragmentation, rather than inhibit it, as had been expected. This was because magnetic tension prevented singularities from arising at the centre of the cloud, which would have ensured the cloud collapsed into a single protostar.

Hosking and Whitworth (2004) performed an SPH simulation which included a two-fluid treatment of ambipolar diffusion. These results were very different from those of Boss (2002) and more in line with conventional wisdom: they found that, even with relatively weak initial field-strength, the presence of magnetic fields prevent fragmentation from occurring. This was because magnetic braking was so effective that it could remove most of the cloud's angular momentum before ambipolar diffusion had reduced the magnetic field strength sufficiently for the cloud to collapse. In this case the strength of ambipolar diffusion was set to what was felt to be a realistic value. When the strength of the ambipolar diffusion was increased (i.e. the coupling between neutral and ionized gases decreased) 25 fold it was found that fragmentation could occur, as magnetic breaking was then much less efficient. However, such a change to the magnitude of ambipolar diffusion is entirely arbitrary and thus its result is

unlikely to have any physical significance.

Despite the fact that Hosking and Whitworth (2004) contradicted his 2002 results Boss stood by them in a letter to MNRAS (2004). Here he asserted that the initial conditions used by Hosking and Whitworth were sufficiently different from his own as to make comparisons invalid. In particular, he claimed that the fragmentation in his 2002 paper was not driven by rotation, whereas that in Hosking and Whitworth (2004) was. Furthermore, he noted that while his simulations included a comprehensive representation of radiative transfer, those of Hosking and Whitworth (2004) used only a simple barotropic equation of state (see below for a discussion of the limitations of such an equation of state) and that this may have been partially responsible for differences between his and their results. However, he acknowledged that until a full MHD simulation could be run which included both ambipolar diffusion and radiative transfer, this would remain an open question (Boss, 2004).

Boss continued to study the collapse of gas clouds into stars using his approximate approach to MHD, examining the evolution of sheet-like (Boss, 2005) and filamentary (Boss, 2007) clouds. Fragmentation was observed in both cases. In the latter paper, Boss introduced a crude representation of magnetic breaking, although this had little effect on the outcome of the simulations. It should be noted, however, that these filamentary clouds only collapsed due to shocks created when outflows were reflected off the boundaries of the simulation. While Boss (2007) suggests that it is possible for a similar effect to be achieved with periodic boundary conditions (i.e. many adjacent filamentary cloud cores), no simulations were conducted to test this.

Shortly after Hosking and Whitworth (2004), Machida et al. (2004) published a

finite-difference 3D simulation of fragmentation featuring full MHD. Using a series of nested grids and an initially cylindrical cloud core, it was found that fragmentation could occur even when magnetic fields were present, although magnetic fields did make it less likely. Fragmentation was observed occurring after a cloud had evolved to become bar- (as in Truelove et al., 1998) or disc-shaped. Like Hosking and Whitworth (2004), a barotropic equation of state was used.

The next year, the results of an extensive set of simulation were published (Machida et al., 2005a,b) using the same numerical methods as in Machida et al. (2004). The first of these papers dealt with the formation of cores within interstellar gas clouds, while the second followed the evolution of these cores into stars. Similar to Machida et al. (2004), fragmentation was observed to occur from bar- and disc-shaped clouds. Disc clouds could only fragment if the magnetic field was weak (or absent), whereas bar clouds could fragment even in the presence of a strong magnetic field so long as they were rotating rapidly enough. Placing the simulations on a magnetic field (B) and angular rotation speed (Ω) parameter space, Machida et al. (2005b) found that (assuming a central density of 2×10^{-20}g cm^{-3} and a temperature of 10K) fragmentation would occur when the following condition was satisfied:

$$\Omega > 2.0 \times 10^{-14} \mathrm{s}^{-1} \left[\left(\frac{B}{1\mu\mathrm{G}} \right)^{1/2} + 0.25 \right].$$

(1.19)

While these simulations did not include ambipolar diffusion, Machida et al. (2005b) did not feel that its inclusion would dramatically alter the results, except perhaps by promoting fragmentation slightly. As a side note, Machida et al. (2005b) felt that

the results of Hosking and Whitworth (2004) were compatible with equation (1.19), while those of Boss (2002) were not.

Also that year, an AMR code featuring MHD, called NIRVANA, was released (Ziegler, 2005). This code also did not include the effects of ambipolar diffusion and used a barotropic equation of state. Various tests involving the collapse and fragmentation of gas clouds were performed and the results of Truelove et al. (1998) and Hosking and Whitworth (2004) were replicated when magnetic fields were absent. While a strong magnetic field was found to inhibit fragmentation, Ziegler found that a weak one would still allow fragmentation. Furthermore, fragments which would otherwise have recombined into a single object would rebound in the presence of weak magnetic fields and remain separate.

(Price and Bate, 2007) performed fragmentation simulations using a new, more accurate, SPH algorithm for dealing with MHD. Once again, this simulation did not include ambipolar diffusion and used a barotropic equation of state. While their results agreed with the majority of previous work in finding that magnetic fields tend to inhibit fragmentation (although not prevent it to the extent seen elsewhere), Price and Bate (2007) noted that it seemed to be magnetic pressure causing this inhibition, with magnetic tension and breaking playing much smaller roles than usually thought. Furthermore, magnetic tension appeared to actually aid fragmentation by "cushioning" fragments and preventing them from recombining. In this regard, their results agree with Boss (2002).

A 2007 review by Goodwin et al. concluded that, while numerical simulations could easily reproduce fragmentation, they could not adequately match the observed

properties of binary stars. In particular, there was difficulty in reproducing the observed distribution of mass ratios and separation distance in multiple star systems as well as the frequency of multiple star systems. While some simulations were able to reproduce some of these properties, none could reproduce all of them. While Goodwin et al. (2007) admit that problems persist with the numerical methods used to perform such simulations, they feel that this is not the main cause of disagreement with the observations. Rather, they suggest it is largely a result of physics being incompletely represented in the simulations. These problems include treatment of angular-moment transport and feedback due to stars and jets. However, the biggest problem identified is in thermal physics, which in general is only represented using a crude barotropic equation of state.

A barotropic equation of state is one in which pressure is a function only of density, taking the form $p = \kappa \rho^\gamma$ where κ is a constant of proportionality and γ is the adiabatic index. With an appropriate value of γ, a barotropic equation of state can be adiabatic, but the converse is not necessarily true; in an adiabatic system, in general $\kappa = \kappa(T)$ (where T is gas temperature) meaning that $p = p(\rho, T)$ and the system is not barotropic. A barotropic equation of state enforces entropy conservation, resulting in unphysical isentropic shocks. It also prevents the spontaneous formation of contact discontinuities, which is unphysical as well.

The first finite-difference simulation to include ambipolar diffusion was published in 2008 (Duffin and Pudritz). Primarily discussing a single-fluid approximation for ambipolar diffusion (see Section 2.3) which was implemented in the FLASH2.5 AMR code, this paper tested the algorithm with a simulation of a collapsing cloud core.

It was found that ambipolar diffusion allowed clouds to collapse which would not be able to do so using ideal MHD. A more thorough analysis of fragmentation simulations using this algorithm was provided by Duffin and Pudritz (2009). Here it was confirmed that ambipolar diffusion would allow systems to fragment which wouldn't be able to under ideal MHD. With ambipolar diffusion and high rotation, even a fairly small (10%) perturbation led to fragmentation. With a more moderate degree of rotation, a much more dramatic perturbation was required (50%). However, their calculations suggested that such a perturbation was eminently achievable within a turbulent cloud. Thus, while ambipolar diffusion alone will not guarantee fragmentation of a moderately rotating core, it would still be possible for a significant number of such cores.

Chapter 2

AMPIBOLAR DIFFUSION

2.1 Magnetohydrodynamics

The physics of fluid dynamics in the presence of magnetic fields (magnetohydrody-
namics, or MHD) can be captured within four equations. As with all fluid dynamics,
for these equations to apply it is required that there be a sufficiently large number
of particles within any volume of interest so that the particles' collision with the
boundary of the volume provides an isotropic pressure. This can be stated more
mathematically as

$$\delta l \ll \mathcal{L} \tag{2.1}$$

where δl is the mean free path of the particles and $\mathcal{L}$ is the smallest length scale of
interest.

In order to incorporate magnetic fields into fluid dynamics an additional and
similar assumption is required. For magnetic fields to have any impact on the fluid,
the fluid must be ionized (a plasma). The charges within this plasma must be spread
evenly on the length scales which are of interest (i.e. the fluid must be neutral overall
on these scales), if MHD is to work. Additionally, it must be assumed that the
charged particles will move into equilibrium with static electric fields within times
much shorter than all other relevant time-scales. This means that any static electric

field within the fluid will be cancelled.

With these assumptions in mind, the equations for MHD are:

$$\frac{\partial \rho}{\partial t} + \nabla \cdot (\rho \boldsymbol{v}) = 0, \qquad\qquad \text{continuity} \qquad (2.2)$$

$$\frac{\partial \boldsymbol{s}}{\partial t} + \nabla \cdot (\boldsymbol{s} \boldsymbol{v}) = -\nabla p - \rho \nabla \phi + \frac{1}{\mu_0} (\nabla \times \boldsymbol{B}) \times \boldsymbol{B}, \qquad \text{momentum} \qquad (2.3)$$

$$\frac{\partial (e_\mathrm{T}^*)}{\partial t} + \nabla \cdot (e_\mathrm{T} \boldsymbol{v}) = -\nabla \cdot \left(p\boldsymbol{v} + \frac{1}{\mu_0} \boldsymbol{B} \times (\boldsymbol{v} \times \boldsymbol{B}) \right), \qquad \text{total energy} \qquad (2.4)$$

$$\frac{\partial \boldsymbol{B}}{\partial t} - \nabla \times (\boldsymbol{v} \times \boldsymbol{B}) = 0, \qquad\qquad \text{induction.} \qquad (2.5)$$

Alternatively, Equation (2.4) can be replaced by

$$\frac{\partial e}{\partial t} + \nabla \cdot (e\boldsymbol{v}) = -p\nabla \cdot \boldsymbol{v}, \qquad \text{internal energy.} \qquad (2.6)$$

The variables are

ρ density of the fluid;

t time;

$\boldsymbol{v}$ velocity (a vector);

$\boldsymbol{s}$ momentum (a vector);

p thermal pressure;

ϕ gravitational potential;

μ_0 permeability of free space;

$\boldsymbol{B}$ magnetic field (a vector);

e internal energy;

e_T total energy ($e_\mathrm{T} = \frac{1}{2}\rho v^2 + e + \rho\phi$);

e_{T}^{*} total energy including the magnetic field ($e_{\mathrm{T}}^{*} = e_{\mathrm{T}} + B^2/2\mu_0$).

These equations describe ideal MHD in which there is assumed to be no viscosity, resistivity and the fluid is completely ionized. In reality, this latter condition often won't be the case. However, as discussed in §1.1.2, it will still serve as a remarkably good approximation, since the ionized component of the gas will be able to drag the neutral component along via collisions. That being said, this by itself will not account for the tendency of magnetic field lines to slip through a partially ionized fluid. For that, one needs to incorporate specifically the process called ambipolar diffusion (A.D.).

2.2   Ambipolar Diffusion

If we wish to represent accurately the fact that not all of the gas is ionized, then we must adapt equations (2.2) to (2.5) to represent two separate fluids: the neutral and the ionized. Our equations then become: (Duffin and Pudritz, 2008)

$$\frac{\partial \rho_{\mathrm{n}}}{\partial t} + \nabla \cdot (\rho \boldsymbol{v}_{\mathrm{n}}) = 0, \qquad \text{continuity, neutral;} \quad (2.7)$$

$$\frac{\partial \rho_{\mathrm{i}}}{\partial t} + \nabla \cdot (\rho \boldsymbol{v}_{\mathrm{i}}) = 0, \qquad \text{continuity, ionized;} \quad (2.8)$$

$$\frac{\partial \boldsymbol{s}_{\mathrm{n}}}{\partial t} + \nabla \cdot (\boldsymbol{s}_{\mathrm{n}} \boldsymbol{v}_{\mathrm{n}}) = -\nabla p_{\mathrm{n}} - \rho_{\mathrm{n}} \nabla \phi - \boldsymbol{f}_{\mathrm{f}}, \qquad \text{momentum, neutral;} \quad (2.9)$$

$$\frac{\partial \boldsymbol{s}_{\mathrm{i}}}{\partial t} + \nabla \cdot (\boldsymbol{s}_{\mathrm{i}} \boldsymbol{v}_{\mathrm{i}}) = -\nabla p_{\mathrm{i}} - \rho_{\mathrm{i}} \nabla \phi + \boldsymbol{f}_{\mathrm{f}}$$

$$+ \frac{1}{\mu_0}(\nabla \times \boldsymbol{B}) \times \boldsymbol{B}, \qquad \text{momentum, ionized;} \quad (2.10)$$

$$\frac{\partial (e_{\mathrm{T,n}})}{\partial t} + \nabla \cdot (e_{\mathrm{T,n}} \boldsymbol{v}_{\mathrm{n}}) = -\nabla \cdot (p_{\mathrm{n}} \boldsymbol{v}_{\mathrm{n}}) - \boldsymbol{v}_{\mathrm{n}} \cdot \boldsymbol{f}_{\mathrm{f}}, \qquad \text{total energy, neutral;} \quad (2.11)$$

$$\frac{\partial(e_{\mathrm{T,i}}^{*})}{\partial t} + \nabla \cdot (e_{\mathrm{T,i}} \boldsymbol{v}_{\mathrm{i}}) = -\nabla \cdot (p_{\mathrm{i}} \boldsymbol{v}_{\mathrm{i}}) + \boldsymbol{v}_{\mathrm{i}} \cdot \boldsymbol{f}_{\mathrm{f}}$$

$$- \nabla \cdot \left(\frac{1}{\mu_0} \boldsymbol{B} \times (\boldsymbol{v}_{\mathrm{i}} \times \boldsymbol{B}) \right), \qquad \text{total energy, ionized;} \quad (2.12)$$

$$\frac{\partial \boldsymbol{B}}{\partial t} - \nabla \times (\boldsymbol{v}_{\mathrm{i}} \times \boldsymbol{B}) = 0, \qquad\qquad\qquad \text{induction;} \quad (2.13)$$

where all variables have the same meaning as in equations (2.2)–(2.5). The subscripts i and n signify that a variable describes only the ionized or neutral gas, respectively. $\boldsymbol{f}_{\mathrm{f}}$ is the frictional force caused by collisions between ionized and neutral particles and is given by (Duffin and Pudritz, 2008 and references therein)

$$\boldsymbol{f}_{\mathrm{f}} \equiv \gamma_{\mathrm{AD}} \rho_{\mathrm{i}} \rho_{\mathrm{n}} (\boldsymbol{v}_{\mathrm{n}} - \boldsymbol{v}_{\mathrm{i}}) = -\frac{1}{\mu_0 \beta_{\mathrm{AD}}} \boldsymbol{v}_{\mathrm{d}} \qquad (2.14)$$

where $\boldsymbol{v}_{\mathrm{d}}$ is defined to be

$$\boldsymbol{v}_{\mathrm{d}} \equiv \boldsymbol{v}_{\mathrm{i}} - \boldsymbol{v}_{\mathrm{n}} \qquad (2.15)$$

and

$$\beta_{\mathrm{AD}} = 1.4/(\mu_0 \gamma_{\mathrm{AD}} \rho_{\mathrm{i}} \rho_{\mathrm{n}}). \qquad (2.16)$$

The strength of the ion-neutral coupling is represented by the drag coefficient $\gamma_{\mathrm{AD}} = (\langle \sigma \omega \rangle)_{\mathrm{ni}}/(m_{\mathrm{i}} + m_{\mathrm{n}}) = 3.28 \times 10^{13}$ $\mathrm{g}^{-1}\mathrm{cm}^3\mathrm{s}^{-1}$, calculated assuming that most ions are Na^+ and HCO^+ which both have a mass of approximately 29.0 amu and a collision rate with molecular hydrogen of approximately $\langle \sigma \omega \rangle_{\mathrm{ni}} = 1.7 \times 10^{-9}$ $\mathrm{cm}^{-3}\mathrm{s}^{-1}$(Duffin and Pudritz, 2008 and references therein). The coefficient of 1.4 in Equation (2.16) arises from the fact that the interstellar medium contains about one helium atom for every hydrogen atom and the coefficient would be equal to 1.0 if only hydrogen were

present.

As in the case of ideal MHD, equations (2.11) and (2.12) can be replaced by their respective internal energy equations:

$$\frac{\partial e_{\mathrm{n}}}{\partial t} + \nabla \cdot (e_{\mathrm{n}} \boldsymbol{v}_{\mathrm{n}}) = -p_{\mathrm{n}} \nabla \cdot \boldsymbol{v}_{\mathrm{n}}, \tag{2.17}$$

$$\frac{\partial e_{\mathrm{i}}}{\partial t} + \nabla \cdot (e_{\mathrm{i}} \boldsymbol{v}_{\mathrm{i}}) = -p_{\mathrm{i}} \nabla \cdot \boldsymbol{v}_{\mathrm{i}}. \tag{2.18}$$

Note however, that no term representing ambipolar diffusion is present in either equation. To derive Equation (2.30), a $\boldsymbol{v} \cdot \boldsymbol{f}_f$ seems to be required on the right hand side of one or both of the above equations. The absence of such a term indicates a problem in how the energy of the fluid is being understood in the context of these derivations.

2.3 Single-Fluid A.D. Approximation

This problem can be greatly simplified by making a single-fluid approximation, following the arguments given by Duffin and Pudritz (2008). A similar approach has been used elsewhere, including Mac Low et al. (1995), Padoan et al. (2000), Chen and Ostriker (2012) and, most recently, within the context of an SPH code by Wurster et al. (2014). If $\rho_{\mathrm{i}} \ll \rho_{\mathrm{n}}$, if the ions are perfectly coupled to the magnetic field, and if the time-scale for ion-neutral collisions is much smaller than other dynamic time-scales, then there will be strong coupling between the neutral and the ion fluids. These conditions allow equations (2.8)–(2.13) to be greatly simplified, resulting in the recovery of a set of equations similar to equations (2.2)–(2.5), but with a few

correction terms for A.D. added.

For short time scales for ion-neutral collisions, all but the frictional and magnetic terms in Equation (2.9) can be ignored, leaving:

$$0 = \boldsymbol{f}_\text{f} + \frac{1}{\mu_0}(\nabla \times \boldsymbol{B}) \times \boldsymbol{B} \quad \Rightarrow \quad \boldsymbol{f}_\text{f} = -\boldsymbol{J} \times \boldsymbol{B} \tag{2.19}$$

where, according to Ampère's Law, the current density is $\boldsymbol{J} = \frac{1}{\mu_0}\nabla \times \boldsymbol{B}$. The Lorentz force is given by

$$\boldsymbol{f}_L = \boldsymbol{J} \times \boldsymbol{B}. \tag{2.20}$$

Comparing this with equations (2.14) and (2.15), it can be seen that $\boldsymbol{v}_\text{d} = \mu_0\beta_\text{AD}\boldsymbol{f}_\text{L}$, implying

$$\boldsymbol{v}_\text{i} = \boldsymbol{v}_\text{n} + \mu_0\beta_\text{AD}\boldsymbol{f}_\text{L}. \tag{2.21}$$

Substituting this into Equation (2.13) yields

$$\frac{\partial \boldsymbol{B}}{\partial t} = \nabla \times (\boldsymbol{v}_\text{n} \times \boldsymbol{B}) + \nabla \times (\mu_0\beta_\text{AD}\boldsymbol{f}_\text{L} \times \boldsymbol{B}), \tag{2.22}$$

while combining equations (2.9) and (2.19) gives

$$\frac{\partial \boldsymbol{s_\text{n}}}{\partial t} + \nabla \cdot (\boldsymbol{s}_\text{n}\boldsymbol{v}_\text{n}) = -\nabla p_\text{n} - \rho_\text{n}\nabla\phi + \frac{1}{\mu_0}(\nabla \times \boldsymbol{B}) \times \boldsymbol{B}. \tag{2.23}$$

Note that Equation (2.23) is mathematically the same as Equation (2.3).

Defining $e^*_\text{T,n} = e_\text{T,n} + B^2/2\mu_0$ and taking the partial derivative with respect to

time results in

$$\frac{\partial(e_{\mathrm{T,n}}^*)}{\partial t} = \frac{\partial e_{\mathrm{T,n}}}{\partial t} + \frac{1}{\mu_0}\boldsymbol{B}\cdot\frac{\partial\boldsymbol{B}}{\partial t} = -\nabla\cdot\left[(e_{\mathrm{T,n}}+p_{\mathrm{n}})\,\boldsymbol{v}_{\mathrm{n}}\right] - \boldsymbol{v}_{\mathrm{n}}\cdot\boldsymbol{f}_{\mathrm{f}} + \frac{1}{\mu_0}\boldsymbol{B}\cdot\frac{\partial\boldsymbol{B}}{\partial t}, \quad (2.24)$$

using Equation (2.11). Now, using equations (2.19) and (2.22) as well as Ampère's law and various vector identities, it can be shown that:

$$
\begin{aligned}
-\boldsymbol{v}_{\mathrm{n}}\cdot\boldsymbol{f}_{\mathrm{f}} + \frac{\boldsymbol{B}}{\mu_0}\cdot\frac{\partial\boldsymbol{B}}{\partial t} &= \boldsymbol{v}_{\mathrm{n}}\cdot(\boldsymbol{J}\times\boldsymbol{B}) + \frac{\boldsymbol{B}}{\mu_0}\cdot\left[\nabla\times\left(\boldsymbol{v}_{\mathrm{n}}\times\boldsymbol{B}+\left(\mu_0\beta_{\mathrm{AD}}\left(\boldsymbol{J}\times\boldsymbol{B}\right)\times\boldsymbol{B}\right)\right)\right] \\
&= \frac{1}{\mu_0}\left[\boldsymbol{v}_{\mathrm{n}}\cdot\left((\nabla\times\boldsymbol{B})\times\boldsymbol{B}\right)+\boldsymbol{B}\cdot\left(\nabla\times(\boldsymbol{v}_{\mathrm{n}}\times\boldsymbol{B})\right)\right] \\
&\quad + \boldsymbol{B}\cdot\nabla\times[\beta_{\mathrm{AD}}(\boldsymbol{J}\times\boldsymbol{B})\times\boldsymbol{B}] \\
&= \frac{1}{\mu_0}\left[\boldsymbol{v}_{\mathrm{n}}\cdot\left((\nabla\times\boldsymbol{B})\times\boldsymbol{B}\right)+\boldsymbol{B}\cdot\left(\nabla\times(\boldsymbol{v}_{\mathrm{n}}\times\boldsymbol{B})\right)\right] \\
&\quad + \nabla\cdot\left[\left(\beta_{\mathrm{AD}}(\boldsymbol{J}\times\boldsymbol{B})\times\boldsymbol{B}\right)\times\boldsymbol{B}\right] + [\beta_{\mathrm{AD}}(\boldsymbol{J}\times\boldsymbol{B})\times\boldsymbol{B}]\cdot(\nabla\times\boldsymbol{B}) \\
&= \frac{1}{\mu_0}\left[\boldsymbol{v}_{\mathrm{n}}\cdot\left((\nabla\times\boldsymbol{B})\times\boldsymbol{B}\right)+\boldsymbol{B}\cdot\left(\nabla\times(\boldsymbol{v}_{\mathrm{n}}\times\boldsymbol{B})\right)\right] \\
&\quad + \nabla\cdot\left[\left(\beta_{\mathrm{AD}}(\boldsymbol{J}\times\boldsymbol{B})\times\boldsymbol{B}\right)\times\boldsymbol{B}\right] + \mu_0\beta_{\mathrm{AD}}\boldsymbol{J}\cdot[(\boldsymbol{J}\times\boldsymbol{B})\times\boldsymbol{B}] \\
&= \frac{1}{\mu_0}\left[\boldsymbol{v}_{\mathrm{n}}\cdot\left((\nabla\times\boldsymbol{B})\times\boldsymbol{B}\right)+\boldsymbol{B}\cdot\left(\nabla\times(\boldsymbol{v}_{\mathrm{n}}\times\boldsymbol{B})\right)\right] \\
&\quad - \nabla\cdot[\beta_{\mathrm{AD}}(\boldsymbol{B}\cdot\boldsymbol{B})(\boldsymbol{J}\times\boldsymbol{B})-\left(\boldsymbol{B}\cdot(\boldsymbol{J}\times\boldsymbol{B})\right)\boldsymbol{B}] \\
&\quad + \mu_0\beta_{\mathrm{AD}}(\boldsymbol{J}\times\boldsymbol{B})\cdot(\boldsymbol{B}\times\boldsymbol{J}) \\
&= -\frac{1}{\mu_0}\left[(\nabla\times\boldsymbol{B})\cdot(\boldsymbol{v}_{\mathrm{n}}\times\boldsymbol{B})-\boldsymbol{B}\cdot\left(\nabla\times(\boldsymbol{v}_{\mathrm{n}}\times\boldsymbol{B})\right)\right] \\
&\quad - \nabla\cdot(\beta_{\mathrm{AD}}B^2\boldsymbol{J}\times\boldsymbol{B}) - \mu_0\beta_{\mathrm{AD}}\|\boldsymbol{J}\times\boldsymbol{B}\|^2 \\
&= -\frac{1}{\mu_0}\nabla\cdot\left(\boldsymbol{B}\times(\boldsymbol{v}_{\mathrm{n}}\times\boldsymbol{B})\right) - \nabla\cdot(\beta_{\mathrm{AD}}B^2\boldsymbol{f}_L) - \mu_0\beta_{\mathrm{AD}}f_L^2.
\end{aligned}
$$

Rearranging Equation (2.24) gives

$$\frac{\partial(e_{\mathrm{T,n}}^*)}{\partial t} + \nabla \cdot (e_{\mathrm{T,n}} \boldsymbol{v}_{\mathrm{n}}) = -\nabla \cdot \left(p_{\mathrm{n}} \boldsymbol{v}_{\mathrm{n}} + \frac{1}{\mu_0} \boldsymbol{B} \times (\boldsymbol{v} \times \boldsymbol{B}) + \beta_{\mathrm{AD}} B^2 \boldsymbol{f}_L \right) - \beta_{\mathrm{AD}} f_L^2. \quad (2.25)$$

Equations (2.7), (2.3), (2.25), and (2.22) completely describe the behaviour of the neutral fluid and the magnetic fields, within the constraints of the single-fluid approximation. As this is the only fluid which it will now be necessary to track, the subscript n will henceforth be omitted. The MHD equations, including ambipolar diffusion, are thus

$$\frac{\partial \rho}{\partial t} + \nabla \cdot (\rho \boldsymbol{v}) = 0, \quad (2.26)$$

$$\frac{\partial \boldsymbol{s}}{\partial t} + \nabla \cdot (\boldsymbol{s} \boldsymbol{v}) = -\nabla p - \rho \nabla \phi + \frac{1}{\mu_0} (\nabla \times \boldsymbol{B}) \times \boldsymbol{B}, \quad (2.27)$$

$$\frac{\partial(e_{\mathrm{T}}^*)}{\partial t} + \nabla \cdot (e_{\mathrm{T}} \boldsymbol{v}) = -\nabla \cdot \left(p\boldsymbol{v} + \frac{1}{\mu_0} \boldsymbol{B} \times (\boldsymbol{v} \times \boldsymbol{B}) + \beta_{\mathrm{AD}} B^2 \boldsymbol{f}_{\mathrm{L}} \right)$$

$$+ \mu_0 \beta_{\mathrm{AD}} f_{\mathrm{L}}^2, [1] \quad (2.28)$$

$$\frac{\partial \boldsymbol{B}}{\partial t} - \nabla \times (\boldsymbol{v} \times \boldsymbol{B}) = \nabla \times (\mu_0 \beta_{\mathrm{AD}} \boldsymbol{f}_{\mathrm{L}} \times \boldsymbol{B}). \quad (2.29)$$

There have been difficulties in determining the internal energy equation for the single-fluid approximation. Attempts to derive it would appear to indicate that it should be the same as Equation 2.17. However, this does not produce the correct

---

[1]The derivation performed in this section indicates that the $\mu_0 \beta_{\mathrm{AD}} f_L^2$ term should be subtracted from the energy equation. However, this disagrees with the result in Duffin and Pudritz (2008), in which the term is added. As $\mu_0 \beta_{\mathrm{AD}} f_L^2$ is positive-definite, subtracting it inevitably results in negative energy densities, which is clearly unphysical. Furthermore, the term must be added, rather than subtracted, in order to produce agreement with known solutions to equations (2.7)–(2.13). Given these considerations, the result for the energy equation as derived by Duffin and Pudritz (2008) was used, although it remains unclear how this result was obtained.

results when used in computer simulations. Those have shown, empirically, that the correct form of the internal energy equation is

$$\frac{\partial e}{\partial t} + \nabla \cdot (e\boldsymbol{v}) = -p\nabla \cdot \boldsymbol{v} - \boldsymbol{v} \cdot \boldsymbol{f}_{\mathrm{L}}. \tag{2.30}$$

The inability to derive this result indicates a flawed understanding of how energy is treated in ambipolar diffusion and should be further investigated in later work.

2.4 Ion Density

Equations (2.26)–(2.29) use the variable β_{AD} to describe the strength of ambipolar diffusion. As can be seen from equation (2.16), this variable depends upon the density of ionized fluid. To calculate this quantity, Duffin and Pudritz (2008) used the parameterization:

$$n_{\mathrm{i}} = 3 \times 10^{-3} \mathrm{cm}^{-3} \left(\frac{n_{\mathrm{n}}}{10^5 \mathrm{cm}^{-3}}\right)^{1/2} + 4.64 \times 10^{-4} \mathrm{cm}^{-3} \left(\frac{n_{\mathrm{n}}}{10^3 \mathrm{cm}^{-3}}\right)^{-2}, \tag{2.31}$$

where n_{i} and n_{n} are the number densities of ions and neutral particles, respectively. A similar parameterization has been used elsewhere, including by Fiedler and Mouschovias (1992, 1993) and by Hosking and Whitworth (2004), the latter of which attribute it to a model developed by Nakano (1976).

When rewritten to provide the mass densities in a scale-free manner, equation

(2.31) becomes

$$\rho_{\rm i} = \sqrt{\frac{9 \times 10^{-11} \text{ cm}^{-3} \, m_{\rm i}^2}{\rho_{\rm s} m_{\rm n}}} \sqrt{\rho_{\rm n}} + 464 \text{cm}^{-9} \frac{m_{\rm n}^2 m_{\rm i}}{\rho_{\rm s}} \frac{1}{\rho_{\rm n}^2}, \tag{2.32}$$

where $m_{\rm i}$ and $m_{\rm n}$ are the masses of the ionized and neutral particles and $\rho_{\rm s}$ is a scaling-factor which converts between density in CGS units and whatever units are to be used for the mass densities ($\rho_{\rm i}$ and $\rho_{\rm n}$). If, for example, one density unit was meant to correspond to atomic hydrogen with $n = 10^6$ cm^{-3}, then $\rho_{\rm s} = 2 \times 10^{-18}$ g cm^{-3}. Note that the particle masses used by Duffin and Pudritz (2008), and for the collapse simulations performed for this thesis, were $m_{\rm i} = 29.0$ amu and $m_{\rm n} = 2.3$ amu.

Chapter 3

NUMERICAL METHODS

3.1 *ZEUS-3D*

The software used to perform the simulations which follow was the *ZEUS-3D* code. This is a grid-based fluid-dynamics code designed for astrophysical applications. It is capable of simulating various types of physics, including MHD and self-gravity. Unusually, *ZEUS-3D* uses what is known as a "staggered-grid" approach. This means that the values of each physical quantity in each zone of the grid are not all located at the same place in the zone. Specifically, scalar quantities are "zone-centred", whereas each component of a vector quantity is located on the corresponding normal face of the zone ("face-centred") (Clarke, 1996). Effectively, the purpose of *ZEUS-3D* is to solve numerically equations (2.2)–(2.5). As part of this research, the code was altered so that, if desired, it could also solve equations (2.26)–(2.29), allowing for ambipolar diffusion. See Appendix A for a detailed description of the implementation.

Ideally, for fragmentation simulations Adaptive Mesh Refinement (AMR) would be use. While a version of *ZEUS-3D* does exist with AMR capabilities (*AZEuS*) and has, in the past, been succesfully used to replicate the results of Truelove et al. (1998) (Ramsey et al., 2012) it currently features only an order N^2 algorithm for self-gravity (compared to the two $N \log N$ algorithms available in *ZEUS-3D*), which would be

prohibitively expensive computationally. Furthermore, serious issues persist regarding the integration of some of *ZEUS-3D*'s new features (in particular, its redesigned transport algorithms) and *AZEuS*'s overly-large memory footprint. As it was unclear if all of these issues could be resolved in time for the writing of this thesis, the decision was made to continue using *ZEUS-3D*, despite the lack of AMR.

For each simulation, the maximum Jeans number was tracked. If, during a simulation, the Jeans number increased beyond 0.25 then nothing in that simulation thereafter can be considered reliable. Effectively, that simulation must be regarded as having been cut short. In order to prevent such a violation of the Jeans condition from occurring, a sufficiently high resolution must be used. Initially, a nonuniform grid was used so as to increase the resolution available for the cloud-fragments. In the inner 40% of the grid there was a uniform resolution approximately 1.7 times finer than had the grid been uniform. Just beyond the edge of this region the zones would have approximately the same size, but grown larger by a geometric progression the closer they were to the edges of the domain. This meant that any fragments could be expected to fall within the highest resolution area, the entire initial gas cloud within a region of at least comparable resolution to what would have existed had the grid been uniform, and the exterior of the gas cloud (which is of little interest) in a lower-resolution region where a minimum of computational resources would be wasted.

As mentioned previously, *ZEUS-3D* features two $N \log N$ self-gravity algorithms. One (`gravfft`) uses Fourier transforms to solve the Poisson equation and, if used in conjunction with the FFTW3 library, can work on arbitrarily-sized grids (although

grids of size 2^n or $2^n - 1$, where n is an integer, can be the most efficiently evaluated, depending on the boundary conditions). That ability means that it will be able to work with *AZEuS* and at some point in time it will be integrated into that code. However, this algorithm requires uniform grids, making it unsuitable for this application. The alternative approach is the full multi-grid algorithm (`gravfmg`). This can be used with nonuniform grids, although there is the minor disadvantage that the number of zones in each dimension must be equal to $2^n - 1$, where n is an integer.

Tests of *ZEUS-3D* indicated that, with uniform grids, the performance (in terms of both accuracy and speed) of `gravfft` and `gravfmg` was comparable. However, further tests revealed that the performance of `gravfmg` declined greatly in terms of speed. This, combined with the fact that `gravfmg` was not amenable to execution with parallel processors, meant that it was actually faster to run a uniform grid simulation with twice the number of zones per dimension using `gravfft`.

ZEUS-3D is capable of solving either the total or the internal energy equations. Numerical errors mean that the former will not be able to give positive definite pressures, while the latter will not be conservative in energy. Generally, the chance of developing negative pressures is considered preferable to non-conservation of energy, so the total energy equation initially was chosen to be used. As discussed in §4.2, these simulations actually worked better when solving for internal energy, so that is the method which was ultimately chosen.

3.2 Time Step Considerations

An explicit finite difference code such as *ZEUS-3D* is subject to the so-called CFL condition (Courant et al., 1928), in which the time step chosen to advance the solution must be less than the so-called CFL limit. Violating this criterion can mean the numerical solution succumbs to dramatic zone-to-zone oscillations, rendering it unstable. Each physical process in the MHD fluid—sound waves, Alfvén waves, advection, etc.—introduces its own CFL limited timescale and, in order to run stably, the time step chosen must be smaller than the smallest of these.

The introduction of ambipolar diffusion requires another CFL time step which, as shown by Mac Low et al. (1995), is given by

$$\tau_{\text{AD}} = \frac{(\Delta x)^2}{4\beta_{\text{AD}}B^2}, \tag{3.1}$$

where Δx is the size of a zone. For most applications, it turns out that τ_{AD} can be one or two orders of magnitude smaller than any other characteristic time scale of the fluid and thus simulations including AD tend to take much longer than simulations without it.

Note that Equation 3.1 differs somewhat from the expression given by Duffin and Pudritz (2008) which, among other things, relies upon, in their words, a "fudge-factor". The Mac Low et al. (1995) formulation was used over that of Duffin and Pudritz (2008) as the former was felt to be more general. Information on the implementation of this time step condition can be found in Appendix A.

3.3 C-Shock A.D. Tests

Having implemented the above single-fluid approximation for ambipolar diffusion in *ZEUS-3D*, it was necessary to test it. There exist relatively few ambipolar diffusion problems for which an analytic solution is known. However, a class of problems which make a useful test for an ambipolar diffusion code are C-shocks. A shock is a stable transition between two equilibrium states in a fluid, which is normally discontinuous. However, in a weakly ionized fluid, a shock can occur where the transition is continuous and this is what is referred to as a C-shock.

Strictly speaking, C-shocks do not have analytic solutions. However, they can be described by systems of ordinary differential equations (ODEs), which can then be solve semi-analytically with a computer. Two such cases were examined, both of which are 1-dimensional: an isothermal and a non-isothermal C-shock. The shocks were tested along each axis to ensure that the implementation was correct in all directions.

3.3.1 Isothermal C-Shock

Because an isothermal gas requires no energy equation, modifications to the energy equation are not tested by an isothermal C-shock problem—only those to the induction equation. As such, an isothermal C-shock is the simpler test to perform. The steady-state solution to this problem is provided by Mac Low et al. (1995). By setting the time derivatives in equations (2.7)–(2.13) to zero, the fluid equations can be

reduced to the single ODE for the dimensionless density $D = \rho/\rho_0$:

$$\left(\frac{1}{D^2} - \frac{1}{M^2}\right) L \frac{dD}{dx} = \frac{\sqrt{2}b}{A} \left[b - D\left(\frac{b - b_0}{A^2} \cos^2\theta + \sin\theta\right)\right] (b^2 + \cos^2\theta)^{-1}, \quad (3.2)$$

where b and D are related by

$$b^2 = b_0^2 + 2A^2(D - 1)(D^{-1} - M^{-2}). \quad (3.3)$$

In these equations, $b = B_y/B_0$ is the dimensionless transverse magnetic field, $M = v_{x,0}/c_\mathrm{s}$ is the thermal Mach number ($v_{x,0}$ is the pre-shock velocity in the x-direction), the Alfvén Mach number is $A = \sqrt{4\pi\rho_0}v_{x,0}/B_0$, and

$$L = \sqrt{2}B_0/(\gamma\rho_\mathrm{i}\sqrt{4\pi\rho_0}) \quad (3.4)$$

is the shock length-scale. ρ_i corresponds to ionized fluid density, whereas ρ represents the neutral fluid density. θ is the angle between the pre-shock velocity ($v_{x,0}$, along the direction of the shock) and magnetic field $\boldsymbol{B}_0$ vectors. The pre-shock density is ρ_0. x- and y-components of the velocity (where the x-direction aligns with that of the shock) are given by

$$v_x = v_{x,0}/D \quad (3.5)$$

$$v_y = \left(K - \frac{B_x B_y}{4\pi}\right) \frac{1}{\rho_0 v_{x,0}}, \quad (3.6)$$

where $K = \rho_0 v_{x,0} v_{y,0} - \frac{B_{x,0} B_{y,0}}{4\pi}$.

Table 3.1: Initial conditions for C-shock tests, both isothermal and non-isothermal. The state refers to whether the conditions are for before or after the shock. In both cases $\gamma_{\mathrm{AD}} = 1.0$ g^{-1}cm^{3}s^{-1}, $c_{\mathrm{s}} = 0.1$ cm s^{-1}, $B_0 = \sqrt{4\pi}$ G, and $\theta = \pi/4$ ($\Rightarrow B_{\mathrm{y},0} = 2.507$ G). $B_x = 2.507$ G throughout. Ion density was held constant at $\rho_{\mathrm{i}} = 10^{-5}$ g cm^{-3}. The neutral gas was taken to be pure hydrogen, so the coefficient in the numerator of equation 2.16 was set to 1.0.

State	ρ [g cm^{-3}]	P [dyn cm^{-2}]	v_x [cm s^{-1}]	v_y [cm s^{-1}]	B_{y} [G]
Pre	1.000	0.0100	5.000	0.000	2.507
Post (iso)	8.045	0.0804	0.621	0.840	23.553
Post (non-iso)	7.976	0.5	0.627	0.830	23.313

The C-shock simulation was initialized in the same way as Duffin and Pudritz (2008). A region of length $4L$ was given pre-shock conditions, followed by an $8L$ length region in the post-shock state, as predicted by the semi-analytic solution described above. The numerical values can be found in Table 3.1, with various other parameters for the simulation provided in that table's caption. Note that the shock velocity $v_{x,0} = 5.000$ cm s^{-1}. The ion density was kept constant at $\rho_{\mathrm{i}} = 10^{-5}$ g cm^{-3} for the C-shock simulations. Zones of size $L/10$ were used and the simulation was run for 5×10^6 s. The left side of the computational domain had an inflow boundary condition, while the right side had an outflow boundary condition.

The error between a value found numerically (q_{n}) and semi-analytically (q_{a}) is given by

$$\epsilon_q = \left| \frac{q_{\mathrm{a}} - q_{\mathrm{n}}}{\max(q_{\mathrm{a}})} \right| \times 100\%, \tag{3.7}$$

as done in Mac Low et al. (1995) and Duffin and Pudritz (2008). A challenge when calculating the semi-analytic solution is that, if $D = 1$ is provided as a boundary condition, the system is in equilibrium and $D = 1$ for all x. It is thus necessary to

perturb D by a factor of $1 + \epsilon$, where ϵ is some small number. However, it is unclear what value of ϵ should be chosen.

One possibility is to use the numerically determined density value in the first active zone of the computational domain as the boundary condition. However, this yielded fairly poor results ($\sim 5\%$ error) because the semi-analytic solution was translated relative to the numerical one. If, on the other hand, a boundary condition was chosen that differed from the numerical one by $\sim 0.02\%$, then this translation was removed. The reason why this offset is needed is unclear. However, it may be related to the fact that the initial conditions for this test do not constitute a steady-state. As a result, transient features developed while the system relaxed to the steady-state, and these could have introduced numerical errors into the simulation. Such errors could have lead the system to settle on a different steady-state than intended—for example, one in which the shock had some velocity relative to the grid. It is not felt that this indicates any fundamental problem with the implementation of A.D.

A comparison between the numerical results for the C-shock, as found with *ZEUS-3D*, and that found from solving the ODE in Equation (3.2) can be found Figure 3.1. As can be seen in the lower portion of each plot, error was kept below 1% across the entire computational domain for all variables, and below 0.5% for most variables.

3.3.2 Non-Isothermal C-Shock

A solution for a non-isothermal C-shock was derived by Duffin and Pudritz (2008), building on various work from the 1980s and 1990s, particularly that of Wardle (1991).
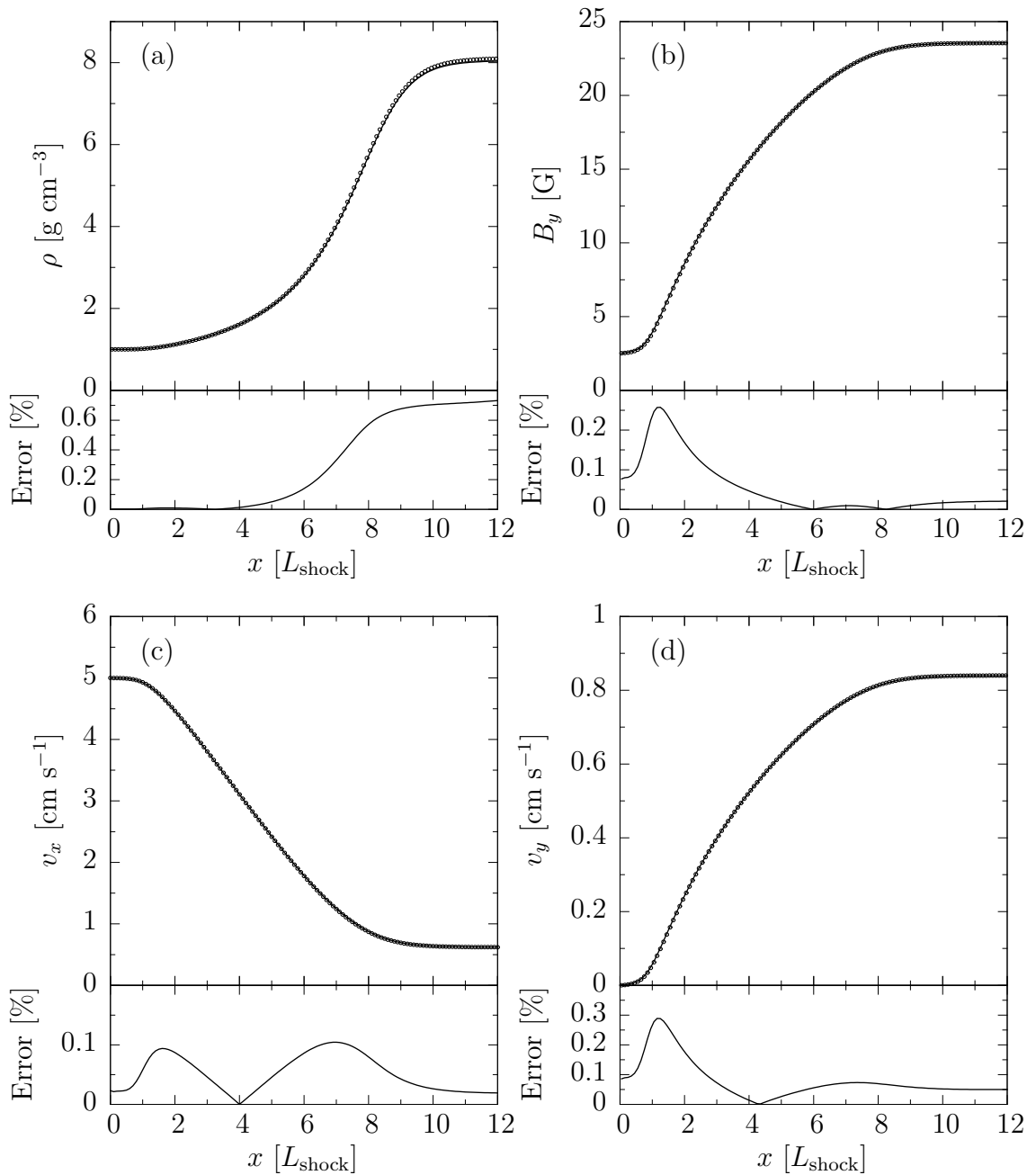
Figure 3.1: Plots comparing the semi-analytic (solid line) solution for an isothermal C-shock to those calculated by *ZEUS-3D* (circles) using the single-fluid approximation discussed in §2.3. The upper portions of the plots show (a) density of the neutral gas, (b) the second component of the magnetic field, (c) the first component of the velocity of the neutral gas, and (d) the second component of the neutral gas velocity. The lower portion of each plot show the level of error in *ZEUS-3D*'s results, as calculated using Equation (3.7).

By setting the time-derivatives to zero in equations (2.7)–(2.13), they found that the steady-state solution for such a C-shock was given by the coupled differential equations

$$\left[\frac{1 - \gamma r_n p}{(\gamma - 1)r_n}\right]\frac{dp}{dz} = \frac{\gamma_{AD}\rho_{i,0}}{v_{x,0}}\left[\left(\frac{1}{r_n} + \frac{\gamma}{\gamma - 1}p - \frac{s_n + \sin\theta}{b}\right)r + \frac{G_n - \Lambda_n}{\gamma_{AD}\rho_{i,0}\rho_0 v_{x,0}^2}\right], \quad (3.8)$$

$$\frac{db}{dz} = \frac{\gamma_{AD}\rho_{i,0}}{v_{x,0}}A^2\left(\frac{r}{b}\right), \quad (3.9)$$

where

$$s_n = \frac{b - b_0}{A^2}\cos^2\theta; \quad (3.10)$$

$$r_n = \frac{1}{1 - (p - p_0) - \left(\frac{b^2 - B_0^2}{2A^2}\right)}; \quad (3.11)$$

$$r_i = r_n\left[\frac{b^2 + \cos^2\theta}{br_n(s_n + \sin\theta) + \cos^2\theta}\right]; \quad (3.12)$$

$$r = 1 - \frac{r_n}{r_i}. \quad (3.13)$$

Here, γ is the adiabatic index, G_n represents heating of the gas as a result of the drift between the ionized and neutral components, and Λ_n is a cooling term added to make the equations more easily integrable numerically. These are given by

$$G_n = \gamma_{AD}\rho_0\rho_{i,0}v_{x,0}^2\frac{r^2}{b^2 r_n}(b^2 + \cos^2\theta) \quad (3.14)$$

$$\Lambda_{\text{AD}} = \begin{cases} \Lambda_{\text{n},0} \left(\frac{\gamma_{\text{AD}} \rho_{\text{i},0}}{v_{x,0}} \right) \left(\frac{p}{p_0} \right), & p > \epsilon_{\text{cool}} p_0 \\ \\ 0, & \text{otherwise} \end{cases} \qquad (3.15)$$

where $\Lambda_{\text{n},0}$ is a normalization factor and ϵ_{cool} defines when the cooling turns on. For this test, the values $\Lambda_{\text{n},0} = 5 \times 10^{-5}$ erg s^{-1} and $\epsilon_{\text{cool}} = 50$ were chosen. The problem was initialized in much the same way as the isothermal C-shock, but using slightly different values for the post-shock state (see Table 3.1).

The results for pressure can be found in Figure 3.2. Once again, it was found that it was necessary to perturb the input data slightly. In this case, a perturbation of 0.6% was able to provide errors of less than 1%, as calculated using Equation (3.7). Figure 3.3 contains plots of B_y and other variables, which were calculated from the following equations, derived from the work of Mac Low et al. (1995):

$$v_x = \left(K_1 - P - \frac{B_y^2}{8\pi} \right) \frac{1}{\rho_0 v_{x,0}}, \qquad (3.16)$$

$$\rho = \frac{\rho_0 v_{x,0}}{v_x}, \qquad (3.17)$$

$$v_y = \left(K_2 + \frac{B_x B_y}{4\pi} \right) \frac{1}{\rho_0 v_{x,0}}, \qquad (3.18)$$

where $K_1 = \rho_0 v_{x,0}^2 + P_0 + \frac{B_{y,0}^2}{8\pi}$ and $K_2 = \rho_0 v_{x,0} v_{y,0} - \frac{B_{x,0} B_{y,0}}{4\pi}$. As before, these requirement of these perturbations is not taken as cause for serious concern, although the required perturbation was larger in this case. Once again, it is not thought that
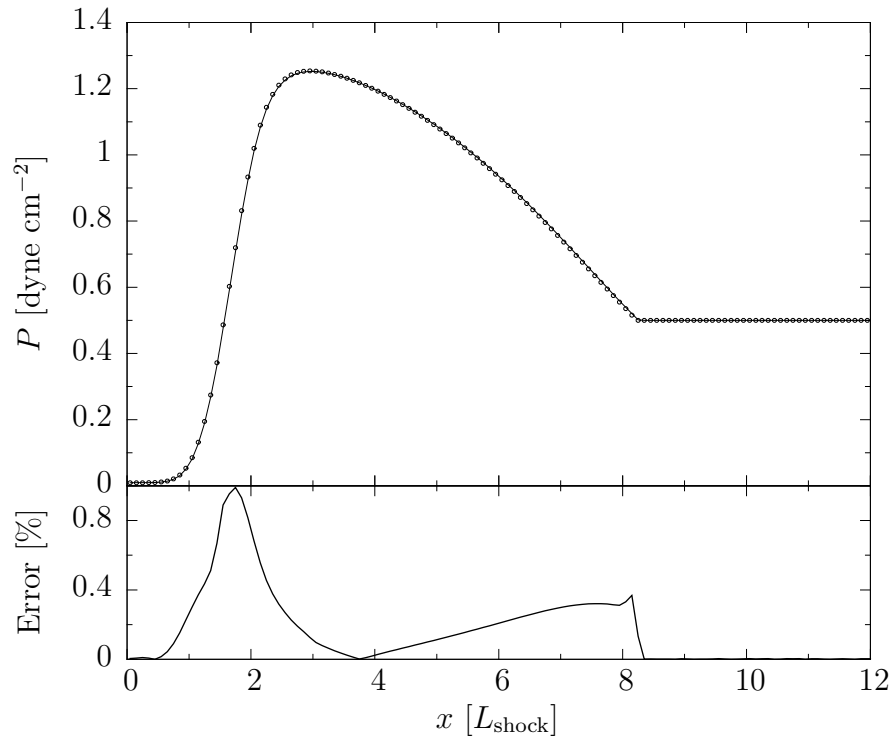
Figure 3.2: A plot comparing the semi-analytic (solid line) solution for pressure in a non-isothermal C-shock to those calculated by *ZEUS-3D* (circles). The upper portion shows these two values for pressure, while the lower portion shows the error in the numerical value, as calculated using Equation (3.7).

the need for this perturbation indicates any major problems with the implementation
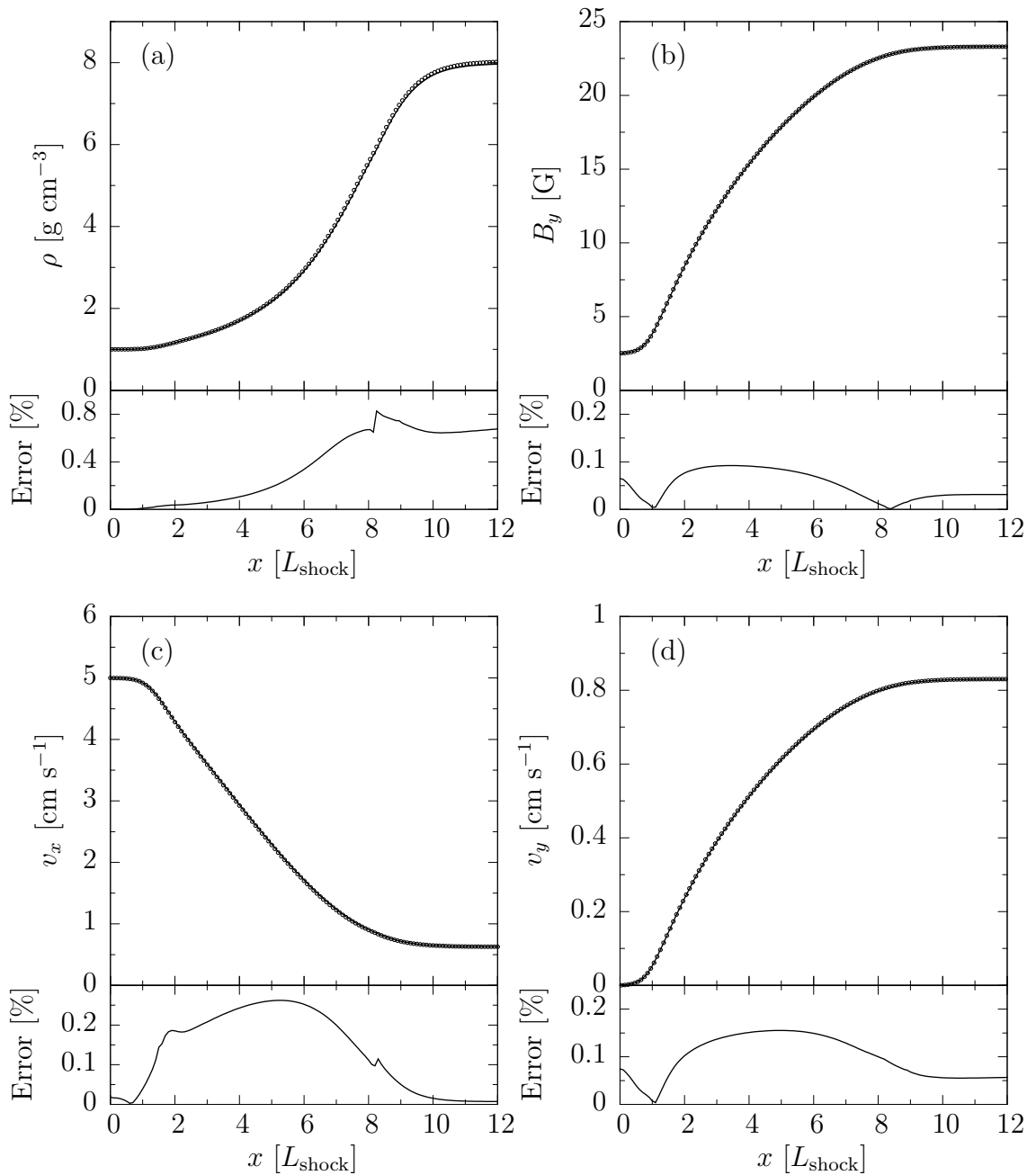
of A.D.

Figure 3.3: Plots comparing the semi-analytic (solid line) solution for a non-isothermal C-shock to those calculated by *ZEUS-3D* (circles) using the single-fluid approximation discussed in §2.3. The upper portions of the plots show (a) density of the neutral gas, (b) the second component of the magnetic field, (c) the first component of the velocity of the neutral gas, and (d) the second component of the neutral gas velocity. The lower portion of each plot show the level of error in *ZEUS-3D*'s results, as calculated using Equation (3.7).

Chapter 4

SIMULATIONS

4.1 Initial Conditions

A uniformly rotating spherical gas cloud was initialized with a mass of $1M_\odot$ and radius $R = 5 \times 10^{16}$ cm. This was centred in a cubical computational domain with edges of size $4R$. The cloud's density was given the perturbation $\rho = \rho_0[1 + 0.1\cos(2\theta)]$ (see Figure 4.1 for an equatorial density slice). A uniform magnetic field threaded the cloud parallel to its axis of rotation. The cloud had parameters $\alpha = 0.3$, $\beta = 0.2$, and $\zeta_\mathrm{m} = 1.0$. The gas surrounding the cloud had the same pressure, but was 100 times less dense. For reasons described in §4.2, it was found that a computational grid with 31^3 zones was the largest size practical, despite the fact that this is extremely low resolution. The simulation was run for a period of $4t_\mathrm{ff}$.

As described in Chapter 1, the collapse of the gas cloud is initially isothermal, but becomes adiabatic as density increases. *ZEUS-3D* is not able to simulate such a transition, so instead the adiabatic index was set to $\gamma = 4/3$, as a compromise between its value for an adiabatic process ($\gamma = 7/5$ for a diatomic gas such as molecular hydrogen) and for an isothermal process ($\gamma = 1$). Outflow boundary conditions were used for MHD variables. The gravitational boundary conditions were preset to be those for a uniform sphere of $1M_\odot$.
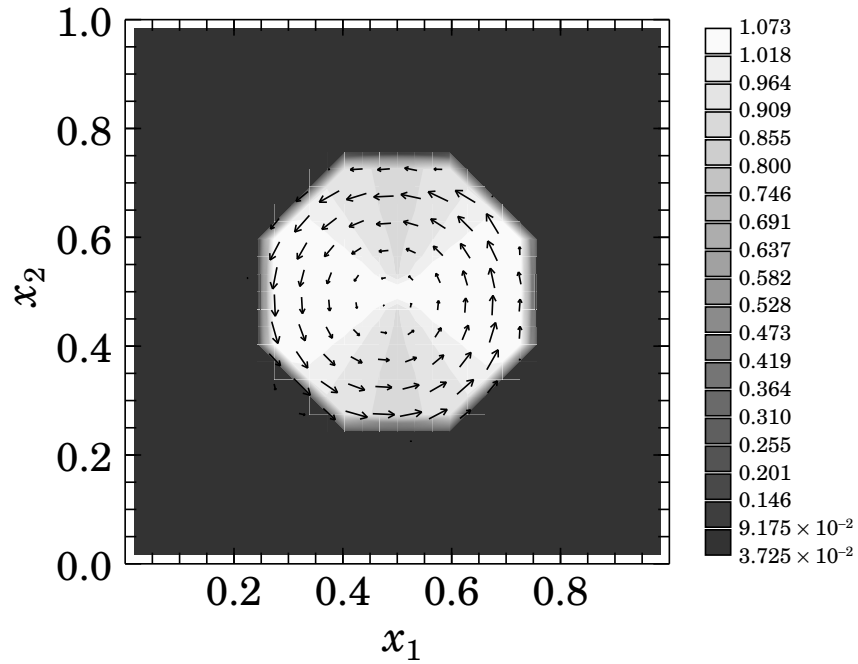
Figure 4.1: An equatorial slice of the computational domain for the initialization of a stellar collapse problem. The colours represent density, while the arrows represent velocity.

Three simulations were performed: one without magnetic fields, one with ideal MHD, and one with ambipolar diffusion. In the latter two simulations, ζ_m was set to 1.0 and the magnetic field was aligned with the axis of rotation. In the case of ambipolar diffusion, ion density was calculated using Equation (2.32), where the ions were Na^+ and HCO^+ ($m_i = 29.0$ amu) and the neutral gas was 90% H_2 and 10% He ($m_n = 2.3$ amu). The value of γ_{AD} was set at $3.28 \times 10^{13} \mathrm{g}^{-1}\mathrm{cm}^3\mathrm{s}^{-1}$, as appropriate for this choice of ionized and neutral species (Duffin and Pudritz, 2008 and references therein).

4.2   Three Dimensional AD

Following the C-shock tests, a low-resolution (31^3 active zones) test-simulation was run of the collapse of a protostellar core with ambipolar diffusion. The initial conditions were the same as those described in §4.1. However, shortly after beginning, the time-step in the simulation began to approach zero. This was found to be due to extreme values for density and pressure (the former very small, the latter very large) occurring in certain zones. Adjusting the parameters of the simulation slightly altered when such an event occurred, but did not prevent its occurrence. The location of the zones determining the time-step would vary with the parameters, but appeared always to be either at a boundary or near the edge of the protostellar core. Investigation with a debugger revealed that an instability developed which began as small perturbations, perhaps caused by round-off error, but grew exponentially until they caused the time-step to approach zero.

An additional issue which was noted was the number of zones in which negative pressures occurred, even for a simulation which was stopped early. While a few occurrences of negative pressure during a simulation are not a problem, a large number tends to indicate some other problem. As a rule of thumb, if the amount of energy which needs to be added in order to reset all pressures to a small positive value is $\lesssim 30\%$ of the total energy in the simulation, then this is not an issue. However, in this case, the amount of energy added was on the order $\gtrsim 10^5\%$.

Further examination of the simulations revealed what appeared to be CFL violations occurring in the regions in which the instabilities described above manifested.
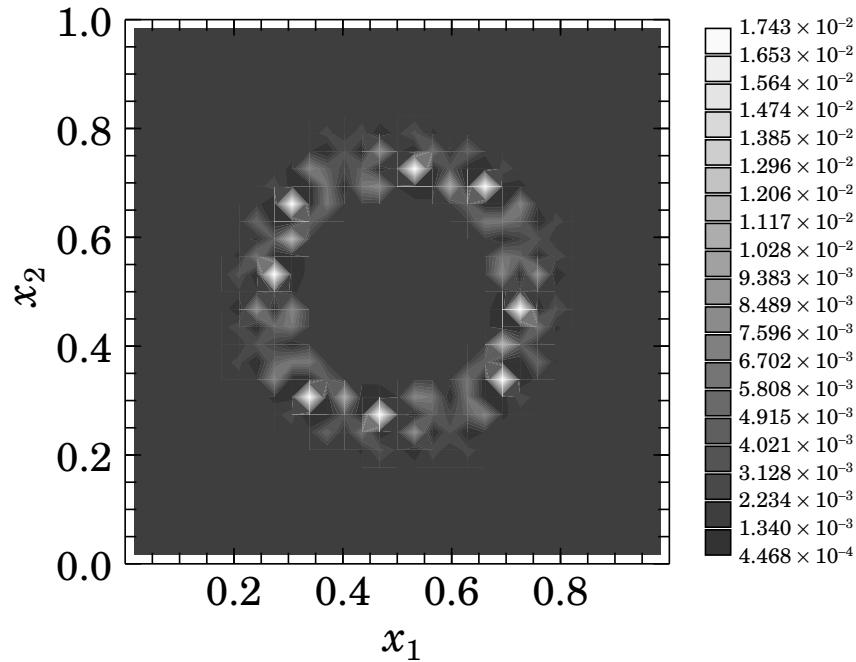
Figure 4.2: A slice of the computational domain for a stellar collapse problem with ambipolar diffusion, early in the simulation. The colours correspond to pressure and the slice is in the plane of the zone which is limiting the time-step. Instabilities, reminiscent of CFL violations, can be seen to form a circle. This circle corresponds to the region just outside the boundary of the protostellar core.

An example of this is shown in Figure 4.2. However, when the time step was artificially reduced, the instabilities persisted. This remained true even when the time-step was reduced by a factor of 1000. This would appear to indicate that the implementation of ambipolar diffusion is inherently unstable. The cause of this instability is unclear, especially as the implementation proved to be successful for the one dimensional C-shock tests.

It was noted that instabilities only ever were observed to arise in regions of low density, outside of the gas cloud. As a stop-gap measure to be able to run a full simulation, the code was modified so that the effects of AD were only applied in zones

(a) $\rho_h = 0.2$ (b) $\rho_h = 0.1$, $\rho_s = 0.2$ (c) $\rho_h = 0.05$, $\rho_s = 0.1$
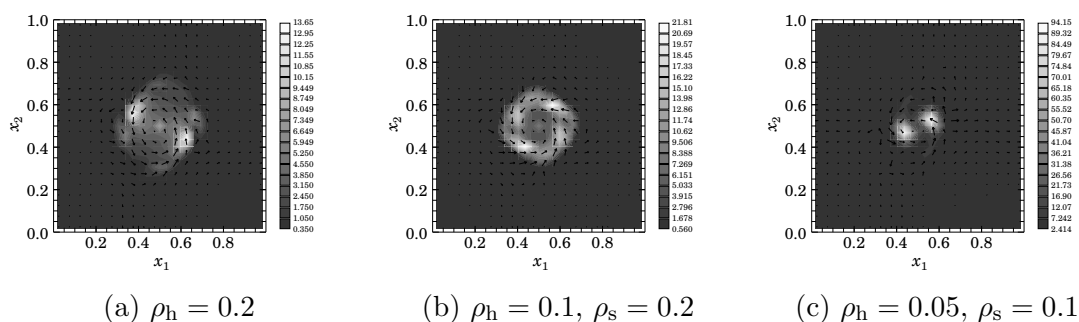
Figure 4.3: Results of a low resolution collapse simulations with different cutoffs for the application of ambipolar diffusion. The grey-scale provides the density, while the arrows show the component of velocity in the plane of the plot. The hard cutoff (ρ_h, below which ambipolar diffusion is not applied at all) and soft cutoff (ρ_s, below which ambipolar diffusion is not applied at full strength) used in each simulation is provided in the caption below its diagram.

with a density above a certain threshold. This modification was later improved so that the application of ambipolar diffusion could be gradually decreased over a range of densities. However, such an approach was ultimately unsuccessful, for multiple reasons. First, while the widespread pattern of instabilities such as that shown in Figure 4.2 did not occur, regions of low density did, nonetheless, develop. These low-density regions would, in the case of the lower cutoffs for the application of ambipolar diffusion, result in the time-step approaching zero more rapidly than the simulation progressed. Thus, the simulation was not able to finish. Furthermore, it was found that different AD cutoffs resulted in qualitatively different results. These results did not converge for any cutoff which allowed the simulation to run to its finish. As such, the accuracy of these simulations is extremely suspect. Finally, this did not resolve the issue of a large number of zones with negative pressures.

As an experiment, the stellar collapse simulation was run with *ZEUS-3D* solving the internal energy equation rather than the total energy equation. This was found

to run without producing any instabilities, even when no cutoff for the application of ambipolar diffusion was used. However, even with ambipolar diffusion turned off, simulations which resulted in fragmentation when run with the total energy equation were found to produce a single object when evaluating the internal energy equation. This may result from the fact that the internal energy equation does not guarantee conservation of energy, causing fragments to move inwards and merge into a single object. Alternatively, it may just be a consequence of the non-linear nature of the problem; changing the algorithm may cause a dramatically different, but no less physical, outcome. Additionally, it should be noted that time constraints prevented the internal energy version of ambipolar diffusion from be tested as thoroughly with C-shocks as was done for the total energy. What limited testing was done indicated that all variables behaved as expected, with the partial exception of pressure. Pressure was found to peak at a lower values than expected and to change slightly more gradually. Again, these are likely to be manifestations of the non-conservative nature of the internal energy transport algorithm. However, despite these issues, it is only with internal energy that 3D simulations could be run with ambipolar diffusion, so it was decided that this was the setting which would be used.

It was found that running simulations with ambipolar diffusion with this resolution took ten hours (in serial). As every doubling in resolution increases the run-time by approximately a factor of 32, this meant that no higher resolution simulation was practical within the time constraints of this thesis, given that problem were experienced when attempting to run *ZEUS-3D* in parallel. Even with parallelism, run-times such as these make ambipolar diffusion impractical to use. Such long run-times

arise because, as noted in §3.2, the characteristic timescale for ambipolar diffusion can be up to two orders of magnitude less than those for other processes. One potential solution to this problem would be to implement AD using sub-cycling. This entails "freezing" the fluid for the length of a relatively long MHD time step, during which time only ambipolar diffusion would be advanced. This would be done at the AD time step, consistent with Equation (3.1). Once enough τ_{rmAD} time steps had elapsed to make up a full MHD time step, the fluid would be unfrozen and allowed to progress through a full MHD time-step. Such an approach has been taken in the past by Mac Low et al. (1995).

4.3   Results

Given that a resolution of only 31^3 could be used in these simulations, their results are of dubious value. Furthermore, the non-linear nature of the stellar collapse problem means that an ensemble of simulations, subjected to statistical analysis, are required in order to draw reliable conclusions. That being said, the three simulations which were run did demonstrate that ambipolar diffusion (AD) produced different results from both MHD and pure hydrodynamics (HD).

An issue which was noted when comparing the simulations was that, after an initial phase of collapses, a rebound occurred. While the initial collapse occurred at roughly the same rate, the rebound and subsequent re-collapse did not. This made it difficult to perform a fair comparison between the end-states of the simulations. As such, it was decided that the simulations would be compared immediately prior to
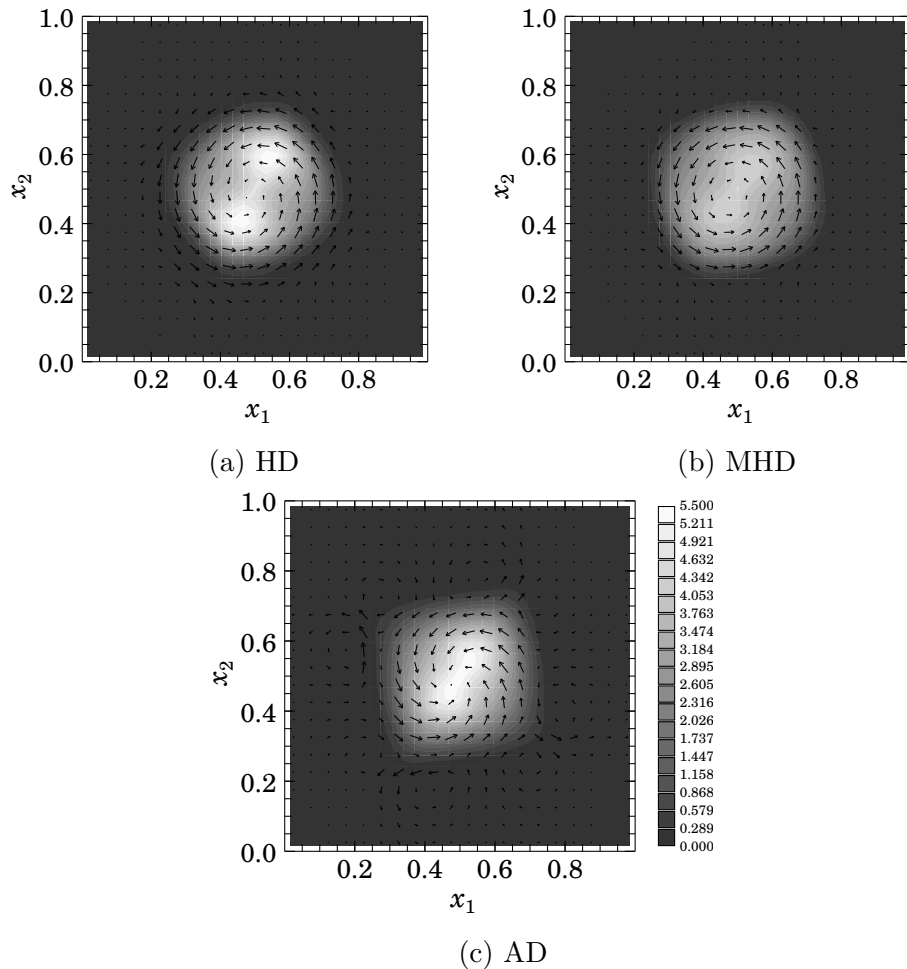
Figure 4.4: The results of the stellar collapse simulations, initialized as described in Section 4.1. Colour indicates density, while arrows indicate velocity in the plane of the plots. The simulations in each plot feature: (a) no magnetic fields, (b) ideal MHD, (c) ambipolar diffusion.

their rebound, at $1t_{\mathrm{ff}}$. The results of the three simulations at that time can be found in Figure 4.3. All simulations met the Jeans condition throughout.

In the HD simulation, two distinct fragments formed, connected by a bar of lower density. In the MHD simulation, however, no such fragments had formed. Instead there was a single, dumbbell-shaped feature. This feature had a much lower density that the fragments seen in the HD simulation. The AD simulation fell between

these two extremes; while it also resulted in a dumbbell-shaped formation rather than separate fragments, the central density of this feature was equal to that of the fragments in the hydrodynamical case.

When a fluid is not ionized (e.g. the HD case) then it will not interact with magnetic fields at all—the field and the fluid will evolve independently. At the other extreme, a fluid which is completely ionized (e.g. the MHD case) will be coupled with the magnetic fields—they evolve together. The magnetic fields are sometimes said to be "frozen" into the fluid, because they will be dragged along with the fluid's motion. As discussed in §1.1.2, ambipolar diffusion represents the intermediate case of partial ionization (e.g. the AD case). The ionized portion of the fluid is coupled with the magnetic field, whereas the neutral component is not (directly). These fluids interact via frictional forces, which transmit some of the effects of the magnetic field to the neutral fluid. Conversely, the friction tends to make the motion of the ionized fluid more similar to that of the neutral one.

This mechanism effectively produces a partial coupling between the neutral component (which, for this single fluid approximation, is several orders of magnitude more dense than the ionized one); the magnetic field will follow the motion of the fluid to some extent, but will tend to drift slightly. Thus, AD represents not only the intermediate case between HD and MHD in terms of amount of ionization, but also in terms of coupling between the fluid and magnetic field. Given this, it was as expected that the AD simulation produced a result displaying characteristics of both the HD and MHD simulations.

Chapter 5

CONCLUSION

This thesis was an attempt to examine the effects of ambipolar diffusion on the collapse and fragmentation of a protostellar core. In order to accomplish this, a single-fluid approximation for ambipolar diffusion, as developed by Duffin and Pudritz (2008), was implemented in *ZEUS-3D*. While this implementation was found to successfully simulate both isothermal and adiabatic C-shocks, it proved to be unreliable for 3D problems. When a protostellar collapse simulation was run with *ZEUS-3D* solving the total energy equation, instabilities developed which mimicked those of CFL violations. However, tests indicated that reducing the time step did not alleviate these instabilities, nor do these instabilities develop when *ZEUS-3D* was run solving the internal energy equation. However, presumably due to this algorithm being non-conservative for energy, fragments tended to recombine into a single object in these simulations. Additionally, ambipolar diffusion required such small time steps that it was impractical to run simulations with even a moderate level of resolution.

The aforementioned difficulties meant that no physical conclusions could be drawn with regard to the collapse and fragmentation of protostellar cores. However, the few simulations which could be run indicated that ambipolar diffusion produced results which were distinctly different from those for ideal MHD and the non-magnetic case. This result fell between those for the latter two simulations; the density was similar

to that obtained in the absence of magnetic fields, while the morphology was closer to that seen in the case of ideal MHD. Such an intermediate result is what would be expected, as the partial ionization resulting in ambipolar diffusion falls between the respective extremes of no ionization and complete ionization.

Much work remains to be done in order to resolve the aforementioned errors. In particular, the cause of the instabilities which arise when *ZEUS-3D* solves for total energy must be identified. The fact that these instabilities do not arise when *ZEUS-3D* solves for internal energy indicates that the implementation of the effects of ambipolar diffusion on induction is correct and that the problem lies with its implementation for energy. There is also the problem of impractical run-times for all but the lowest resolutions. It seems that the implementation of ambipolar diffusion will have to be altered so as to use sub-cycling. This will allow energy and magnetic fields to be updated as necessary, without having to carry out a computationally expensive full iteration of the simulation each time.

Once this has been done, *ZEUS-3D* can be used to evaluate the effects of ambipolar diffusion far more effectively. This will require a much larger set of simulations, run with a variety of different parameters, so as to ensure that any sudden changes in the results due to the nonlinearity of this problem are identified. This will also require a statistical analysis of the results. Ultimately, ambipolar diffusion should be implemented in *AZEuS*, so that these simulations can be run with adaptive mesh refinement, guaranteeing that the Jeans condition is met at all times and allowing much greater detail to be resolved in a computationally cost-effective way.

Appendix A

Implementation of A.D. in *ZEUS-3D*

Note: This appendix assumes a certain amount of knowledge regarding the *ZEUS-3D* code. Readers may find it helpful to first examine *ZEUS-3D*'s manual, which can be downloaded with the source-code at `http://www.ica.smu.ca/zeus3d/`.

The single-fluid approach to ambipolar diffusion described in Chapter 2 results in the addition of an extra term to the induction equation and two extra terms to the energy equation (or, alternatively, an additional term to the internal energy equation). All of these terms involve the Lorentz force $\boldsymbol{f}_L = \boldsymbol{J} \times \boldsymbol{B}$, meaning that this quantity must be calculated. Despite the fact that the information contained by the Lorentz force is used in the MHD calculations performed by *ZEUS-3D*, it has not been explicitly calculated.

With the application of various vector identities, it can be seen that the equation for the kth components of the Lorentz force is given by

$$f_{\text{L},k} = \partial_i(B_i^* B_k^*) + \partial_j(B_j^* B_k^*) + \tfrac{1}{2}\partial_k(B_k^2 - B_j^2 - B_i^2), \qquad (\text{A.1})$$

where $\partial_i \equiv \frac{\partial}{\partial x_i}$ and values with an asterisk are interpolated. In the context of *ZEUS-3D*, interpolation implies more than a simple two-point average. In order to correctly
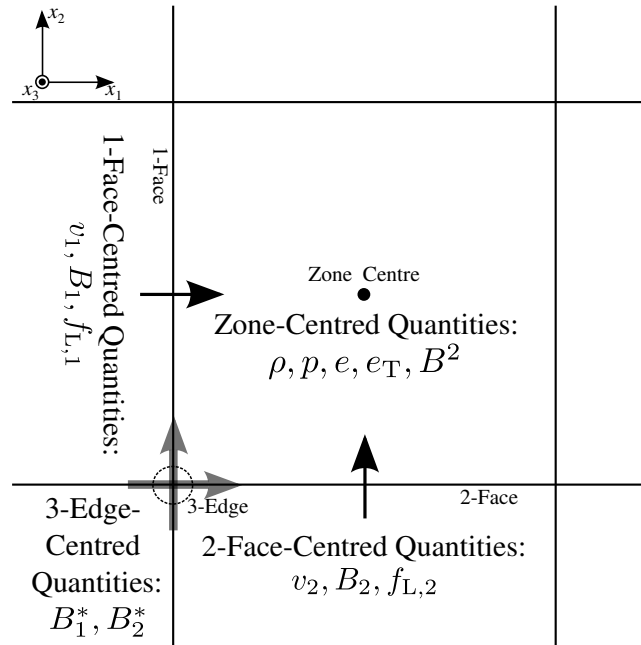
Figure A.1: A cross-section of the *ZEUS-3D* grid, illustrating the location of zone-centred, face-centred, and edge-centred quantities.

account for the propagation of characteristic waves through the fluid, a more complex technique must be used, incorporating concepts such as "upwinding" (Clarke, 1996). $f_{\mathrm{L},k}$ is a face-centred quantity (centred on the k-edge), the interpolated values are edge-centred, and the squared values are zone-centred (see Figure A.1).

As much as possible, terms in Equation (A.1) were used as they were calculated for other purposes. The only exception to this is $\frac{1}{2}\partial_k(B_k^2)$, which was calculated using a new subroutine, `adinit`, at the beginning of `srcstep`. This provided the initial values to store in the Lorentz force arrays (`lz`k, stored in common-deck `ambicom`) for that time-step. The remaining Lorentz force terms were calculated over the course of the transport step. Note that this was only implemented in the newer "resequenced" transport subroutines and not in the deprecated "legacy" transport subroutines. $\frac{1}{2}\partial_k(B_j^2 + B_i^2)$ is then subtracted from (`lz`k) in subroutine `stv`k. Cal-

culation of all of these squared values involved taking a two-point average to obtain the zone-centred value of the magnetic field and then squaring this average. The first derivative of a zone-centred value was then naturally face-centred. The $\partial_i(B_i^* B_k^*)$ term was added to lz$k$ in subroutine ttran$j$, where the interpolated values were already being used. Similarly, $\partial_j(B_j^* B_k^*)$ was added in ttran$i$ The derivative of the edge-centred interpolated values was naturally face-centred. It can be seen how the remaining components of the Lorentz force were calculate by cyclically commuting the indices i, j, and k in the description above.

The effects of ambipolar diffusion were applied in the new subroutine `adapply`, called immediately after the last `ttran*` call in `trnsprt`. At various times the value of β_{AD} was required and this was calculated using a function `beta(dnsty)` where `dnsty` is the density for use in the calculation. Before calculating the $\nabla \cdot (\beta_{\mathrm{AD}} B^2 \boldsymbol{f}_{\mathrm{L}})$ term in the energy equation, B^2 (zone-centred) must be calculated. This involves a two-point average to correctly centre each component of the magnetic field. Next, $\beta_{\mathrm{AD}} B^2 \boldsymbol{f}_{\mathrm{L}}$ (a face-centred quantity) was calculated for each component of $\boldsymbol{f}_{\mathrm{L}}$, taking a two-point average of B^2 in the direction corresponding to the desired component. The face-centred value of density was also calculated for use in determining β_{AD}. The derivative of each component of $\beta_{\mathrm{AD}} B^2 \boldsymbol{f}_{\mathrm{L}}$ was then taken (returning a zone-centred value) and, after multiplying by the time-step dt, subtracted from the total energy. The other A.D. term in the energy equation, $\mu_0 \beta_{\mathrm{AD}} f_{\mathrm{L}}^2$, simply required calculating the sqauare of the Lorentz force (in the same way that B^2 was calculated earlier) and calling `beta` with the normal zone-centred density as the argument. The result, multiplied by dt, could then be added to the total energy.

If *ZEUS-3D* is to be run with `itote == 0` (tracking internal, rather than total, energy) then the calculation is considerably simpler. Only a single term, $\boldsymbol{v}\cdot\boldsymbol{f}_{\mathrm{L}}$ must be added to the internal energy. For each component of $\boldsymbol{v}$ and $\boldsymbol{f}_{\mathrm{L}}$, this was implemented by finding the zone-centred value using a two-point average and taking the product. The product for each component was then added to the internal energy.

Applying ambipolar diffusion to the magnetic fields was the most difficult. Recall that A.D. requires the addition of the term $\nabla \times (\mu_0 \beta_{\mathrm{AD}} \boldsymbol{f}_{\mathrm{L}} \times \boldsymbol{B})$ to the right hand side of the induction equation. The curl must be calculated with care in order to ensure that the solenoidal condition is met. To do this, edge-centred $\boldsymbol{\eta} = \beta_{\mathrm{AD}} \boldsymbol{f}_{\mathrm{L}} \times \boldsymbol{B}$ values were calculated, analogous to electromotive forces (EMFs) calculated when evaluating the unmodified induction equation. Note that, in *ZEUS-3D*, μ_0 is ignored; it is effectively contained within the scaling of the magnetic field. When calculating each component of $\boldsymbol{\eta}$, a four-point average was performed on density to make it edge-centred and from that to calculated β_{AD}. Two-point averages were performed on the relavent components of $\boldsymbol{f}_{\mathrm{L}}$ and $\boldsymbol{B}$ to make them edge-centred as well. In order to ensure that the appropriate boundary conditions are met, skin values (those face-centred values falling between active zones and boundary zones) were set with calls to `svalemf*`. Finally, each component of $\boldsymbol{\eta}$ was passed to the subroutine `ct` (a component of the legacy transport system, where it would normally be passed EMF values) which applied them to the magnetic field. `ct` was designed to correctly handle boundary conditions with a call to subroutine `bvalemfs`. A slight modification to the latter subroutine was needed so that, when it was being used for ambipolar diffusion, it would handle inflow conditions correctly. Ordinarily, `bvalemfs` would set EMFs for

inflow boundaries from active zones or arrays of custom values. However, for A.D., these values should simply be set to zero. For this purpose, a flag `eorn` was added to the argument list of `bvalemfs` (and `ct`, so that the correct value could be passed to `bvalemfs`) which would be set to 1 if EMFs were being passed and any other number of $\boldsymbol{\eta}$ components were being passed for the purposes of ambipolar diffusion.

The time-step required to prevent CFL-violations for ambipolar diffusion is given by Equation (3.1). As done for other conditions limiting the time-step, the inverse square of τ_{AD} was computed for each zone in `newdt`. This was added, in quadrature, with the inverse squares of the other time-step components for that zone and the maximum such value was found. The Courant number (which describes the maximum fraction of material within a cell is allowed to flow out during a time-step) was then divided by the square-root of this result to give the final time-step value. This was the same approach which has always been taken in *ZEUS-3D* to determine the time-step. The only change was that τ_{AD}^{-2} was added to the quadrature sum.

A second implementation of ambipolar diffusion was also added, which treated it as a source term. This meant that the Lorentz force was calculated all at once in the new subroutine `adlf`. This subroutine is called in `srcstep`, immediately before where the diffusive terms are applied when *ZEUS-3D* is run in TWOFLUID mode. A call is made to `adapply` just after `adlf`. This approach worked well for the 1D C-shock simulations, but was found to result in asymmetries when run in 3D. The origin of these asymmetries remains unclear, and this implementation requires further development. This implementation, if perfected, has the advantage of being better suited for subcycling.

As mentioned in Chapter 4, when ambipolar diffusion was applied to the 3D Truelove problem, it was found to cause what appeared to be CFL violations, no matter how small the time-step was reduced. It would seem that the implementation of ambipolar diffusion described here is unconditionally unstable, although why this would be the case for 3D problems but not 1D is unclear. However, it was noticed that such instabilities arose only in the low-density regions external to the gas cloud. As a temporary measure to fix this problem, ambipolar diffusion can be turned off in regions below a certain density. This is achieved by having the function `beta` return a value of zero when its density falls below the desired value, `dminad`. It is also possible to gradually reduce the strength of ambipolar diffusion (i.e. scale the value returned by `beta`) when the density is above `dminad` but below another value, `dmin2ad`. However, these approaches were not successful.

Several parameters may be chosen by the user to control ambipolar diffusion. to override the default values, these parameters must be specified in the namelist `hycon` in the *ZEUS-3D* input file (inzeus):

`adsrc` A switch which, if set to 1, causes Lorentz forces to be calculated all at once and then applied as a source term. This mode contains bugs and should not be used. If set to 0, then the Lorentz forces are calculated over the course of the transport step (default).

`ionconst` A switch which, if set to 1, gives a constant ion density, set to the value of `dscale`. If 0, the ion density is calculated using Equation (2.32) (default).

`gammaad` The coefficient γ_{AD} expressing the strength of the coupling between the

ionized and neutral fluids. Used to calculate β_{AD} in Equation (2.16). (Default: 1.0)

betacoef The coefficient in the numerator of Equation (2.16). It should be 1.4 (default) for a 90% H_2/10% He gas and 1.0 for a pure H_2 gas.

dscale A conversion between scale-free density units used internally by *ZEUS-3D* and cgs density. (Default: 2.0×10^{-18} g cm^{-3})

mion Average mass of ionized particles, in cgs units. (Default: 4.81×10^{-23} g)

mneutral Average mass of neutral particles, in cgs units. (Default: 3.82×10^{-24} g)

dminad A cutoff density, below which ambipolar diffusion will not be applied. This is achieved by setting $\beta_{\mathrm{AD}} = 0$ in such regions. (Default: 0)

dmin2ad A cutoff below which ambipolar diffusion is not applied at full strength. The value of β_{AD} is scaled between 0 and 1 as density varies from dminad and dmin2ad, respectively. (Default: 0)

Bibliography

W. Benz. 3D models of rotating magnetic gas clouds. I - Time evolution, mass spectrum and angular momentum. A&A, 139:378–388, October 1984.

M. J. Berger and P. Colella. Local adaptive mesh refinement for shock hydrodynamics. *Journal of Computational Physics*, 82:64–84, May 1989.

M. J. Berger and J. Oliger. Adaptive Mesh Refinement for Hyperbolic Partial Differential Equations. *Journal of Computational Physics*, 53:484–512, March 1984.

A. P. Boss. Collapse and fragmentation of molecular cloud cores. I - Moderately centrally condensed cores. ApJ, 410:157–167, June 1993.

A. P. Boss. Collapse and Fragmentation of Molecular Cloud Cores. V. Loss of Magnetic Field Support. ApJ, 483:309–319, July 1997.

A. P. Boss. Protostellar Fragmentation Enhanced by Magnetic Fields. ApJ, 545: L61–L64, December 2000.

A. P. Boss. Collapse and Fragmentation of Molecular Cloud Cores. VII. Magnetic Fields and Multiple Protostar Formation. ApJ, 568:743–753, April 2002.

A. P. Boss. On the fragmentation of magnetized cloud cores. MNRAS, 350:L57–L60, May 2004.

A. P. Boss. Collapse and Fragmentation of Molecular Cloud Cores. VIII. Magnetically Supported Infinite Sheets. ApJ, 622:393–403, March 2005.

A. P. Boss. Collapse and Fragmentation of Molecular Cloud Cores. IX. Magnetic Braking of Initially Filamentary Clouds. ApJ, 658:1136–1143, April 2007.

A. P. Boss and P. Bodenheimer. Fragmentation in a rotating protostar - A comparison of two three-dimensional computer codes. ApJ, 234:289–295, November 1979.

B.W. Carroll and D.A. Ostlie. *An Introduction to Modern Astrophysics*. Pearson Addison-Wesley, 2007.

C.-Y. Chen and E. C. Ostriker. Ambipolar Diffusion in Action: Transient C Shock Structure and Prestellar Core Formation. ApJ, 744:124, January 2012.

D. A. Clarke. A Consistent Method of Characteristics for Multidimensional Magnetohydrodynamics. ApJ, 457:291, January 1996.

R. Courant, K. Friedrichs, and H. Lewy. Über die partiellen Differenzengleichungen der mathematischen Physik. *Mathematische Annalen*, 100:32–74, 1928.

E. Dorfi. 3D models for self-gravitating, rotating magnetic interstellar clouds. A&A, 114:151–164, October 1982.

D. F. Duffin and R. E. Pudritz. Simulating hydromagnetic processes in star formation: introducing ambipolar diffusion into an adaptive mesh refinement code. MNRAS, 391:1659–1673, December 2008.

D. F. Duffin and R. E. Pudritz. The Early History of Protostellar Disks, Outflows, and Binary Stars. ApJ, 706:L46–L51, November 2009.

R. A. Fiedler and T. C. Mouschovias. Ambipolar diffusion and star formation: Formation and contraction of axisymmetric cloud cores. I - Formulation of the problem and method of solution. ApJ, 391:199–219, May 1992.

R. A. Fiedler and T. C. Mouschovias. Ambipolar Diffusion and Star Formation: Formation and Contraction of Axisymmetric Cloud Cores. II. Results. ApJ, 415: 680, October 1993.

S. P. Goodwin, P. Kroupa, A. Goodman, and A. Burkert. The Fragmentation of Cores and the Initial Binary Population. *Protostars and Planets V*, pages 133–147, 2007.

J. G. Hosking and A. P. Whitworth. Fragmentation of magnetized cloud cores. MNRAS, 347:1001–1010, January 2004.

F. Hoyle. On the Fragmentation of Gas Clouds Into Galaxies and Stars. ApJ, 118: 513, November 1953.

C. Hunter. The Instability of the Collapse of a Self-Gravitating Gas Cloud. ApJ, 136:594, September 1962.

R. B. Larson. Calculations of three-dimensional collapse and fragmentation. MNRAS, 184:69–85, July 1978.

Z.-Y. Li, R. Banerjee, R. E. Pudritz, J. K. Jørgensen, H. Shang, R. Krasnopolsky, and A. Maury. The Earliest Stages of Star and Planet Formation: Core Collapse, and the Formation of Disks and Outflows. *ArXiv e-prints*, January 2014.

M.-M. Mac Low, M. L. Norman, A. Konigl, and M. Wardle. Incorporation of ambipolar diffusion into the ZEUS magnetohydrodynamics code. ApJ, 442:726–735, April 1995.

M. N. Machida, K. Tomisaka, and T. Matsumoto. First MHD simulation of collapse and fragmentation of magnetized molecular cloud cores. MNRAS, 348:L1–L5, February 2004.

M. N. Machida, T. Matsumoto, K. Tomisaka, and T. Hanawa. Collapse and fragmentation of rotating magnetized clouds - I. Magnetic flux-spin relation. MNRAS, 362:369–381, September 2005a.

M. N. Machida, T. Matsumoto, T. Hanawa, and K. Tomisaka. Collapse and fragmentation of rotating magnetized clouds - II. Binary formation and fragmentation of first cores. MNRAS, 362:382–402, September 2005b.

T. Nakano. Fragmentation of magnetic interstellar clouds by ambipolar diffusion. I. PASJ, 28:355–369, 1976.

P. Padoan, E. Zweibel, and Å. Nordlund. Ambipolar Drift Heating in Turbulent Molecular Clouds. ApJ, 540:332–341, September 2000.

G. J. Phillips. Three-dimensional numerical simulations of collapsing, isothermal magnetic gas clouds. MNRAS, 221:571–587, August 1986a.

G. J. Phillips. Three-dimensional numerical simulations of collapsing isothermal magnetic gas clouds - Non-uniform initial fields. MNRAS, 222:111–119, September 1986b.

D. J. Price and M. R. Bate. The impact of magnetic fields on single and binary star formation. MNRAS, 377:77–90, May 2007.

R. E. Pudritz. Clustered Star Formation. In T. Montmerle and P. André, editors, *From Darkness to Light: Origin and Evolution of Young Stellar Clusters*, volume 243 of *Astronomical Society of the Pacific Conference Series*, page 3, 2001.

J. P. Ramsey, D. A. Clarke, and A. B. Men'shchikov. AZEuS: An Adaptive Zone Eulerian Scheme for Computational Magnetohydrodynamics. ApJS, 199:13, March 2012.

J. E. Tohline. Fragmentation of rotating protostellar clouds. ApJ, 235:866–881, February 1980a.

J. E. Tohline. The gravitational fragmentation of primordial gas clouds. ApJ, 239:417–427, July 1980b.

J. K. Truelove, R. I. Klein, C. F. McKee, J. H. Holliman, II, L. H. Howell, and J. A. Greenough. The Jeans Condition: A New Constraint on Spatial Resolution in Simulations of Isothermal Self-gravitational Hydrodynamics. ApJ, 489:L179–L183, November 1997.

J. K. Truelove, R. I. Klein, C. F. McKee, J. H. Holliman, II, L. H. Howell, J. A. Greenough, and D. T. Woods. Self-gravitational Hydrodynamics with Three-dimensional Adaptive Mesh Refinement: Methodology and Applications to Molecular Cloud Collapse and Fragmentation. ApJ, 495:821–852, March 1998.

M. Wardle. Instability in oblique C-type shocks. MNRAS, 251:119–127, July 1991.

J. Wurster, D. Price, and B. Ayliffe. Ambipolar diffusion in smoothed particle magnetohydrodynamics. MNRAS, 444:1104–1112, October 2014.

U. Ziegler. Self-gravitational adaptive mesh magnetohydrodynamics with the NIR-VANA code. A&A, 435:385–395, May 2005.